ENHANCED PALEOSEISMIC SUCCESSION AT THE CONCUD FAULT (IBERIAN CHAIN, SPAIN): NEW INSIGHTS FOR SEISMIC HAZARD ASSESSMENT

José L. Simón*, Luis E. Arlegui, Lope Ezquerro, Paloma Lafuente, Carlos L. Liesa, Aránzazu Luzón

Dpt. Ciencias de la Tierra, Universidad de Zaragoza, C/ Pedro Cerbuna 12, 50009 Zaragoza, Spain.

* Corresponding author: Tel.: +34 976 76 10 95; fax: +34 976 86 11 06.

E-mail addresses: jsimon@unizar.es (J.L. Simón), arlegui@unizar.es (L.E. Arlegui), lope@unizar.es (L. Ezquerro), palomalt@unizar.es (P. Lafuente), carluis@unizar.es (C.L. Liesa), aluzon@unizar.es (A. Luzón).

Abstract

A new trench excavated at the southern sector of the Concud Fault provided evidence of three paleoseismic events dated to ca. 21 ka, 18 ka, and 13 to 3 ka BP, respectively. The two youngest ones had not been detected in previous studies. The results extend the total recorded paleoseismic succession for the fault: eleven events since ca. 74 ka BP to the present day, with an average recurrence period between 7.1 ± 3.5 and 8.0 ± 3.3 ka; total net accumulated slip of about 20.5 m, with average coseismic slip of 1.9 m. The displacement pattern shows alternating periods of fast slip (up to 0.53 mm/a) and slow slip (0.13 mm/a), resulting in average slip rate of 0.29 mm/a. Using this paleoseismic information, as well as the potential magnitude previously attributed to the characteristic earthquake at the Concud Fault (M ≈ 6.5-6.6), a simple probabilistic seismic hazard analysis has been performed. The estimated probability of occurrence of the characteristic earthquake within the next 500-year period ranges from 2.3% to 26.1%, according to distinct hypotheses on the elapsed time derived from the uncertainty about the age of the youngest event.

Keywords

Concud Fault, Iberian Chain, active tectonics, paleoseismology, seismic hazard, intraplate seismicity

1. Introduction

A common approach for assessing seismic hazard passes through the accurate modelling of past seismic patterns, driven by the assumption that large, characteristic seismic events represent ruptures of the same fault segment with the same coseismic slip and hence the same magnitude (Schwartz and Coppersmith 1984). Given long-term strain rate and constant stress distribution, it follows that characteristic earthquakes would occur at approximately equal intervals. This pattern permits to apply conditional probability procedures that, in turn, provide the likelihood that such an event will occur within a discrete time window (Schwartz and Coppersmith 1984; Yeats et al. 1997).

One of the requirements to perform this procedure is to know the date of the latest seismic event (*elapsed time*). In areas of intense seismicity, low recurrence intervals guaranty that the instrumental, at the worst the historical, record will provide the needed date. On the contrary, regions of low seismicity show larger recurrence intervals and this may imply very well that the latest event could be older than the existing records. This is the case of most intraplate areas, where active faults have large recurrence periods (in the order of 10^3 years; Liu and Zoback 1997) that are seldom considered in seismic hazard assessment. In such regions, studying the geological record for detecting and dating large ancient quakes by means of paleoseismological methods is therefore a critical task (Allen 1986; McCalpin 1996; Yeats et al. 1997).

The Iberian Chain, an intraplate range in eastern Spain, contains a number of active, geologically well-documented faults. The most important ones belong to the intra-mountain Jiloca Graben (Calamocha, Sierra Palomera and Concud faults) and Teruel Graben (El Pobo, Teruel and Valdecebro faults) (Figs. 1 and 2).

Nevertheless, historical and instrumental seismicity of this region is low to moderate (Fig. 2). Epicentres are concentrated (i) close to its western margin; (ii) in the relay zone between Concud and Sierra Palomera faults; (iii) in the Albarracín massif, W of the graben, and (iv) in the area south of Teruel. No significant epicentre clustering occurs along the Concud Fault. Measured magnitudes (Mb) usually range from 1.5 to 3.5, with maximum Mb = 4.4 in the Teruel Graben and Mb = 3.8 in the Albarracín massif (data from IGN 2010). Before the instrumental period, intensities up to VI-VII were recorded in the Albarracín massif (1848), IV-V in the Jiloca Graben (1828), and VIII in the southern Teruel Graben (1656) (Mezcua and Martínez-Solares 1983). Focal depths are always less than 25 km, and typically range from 5 to 15 km. This depth corresponds to the brittle layer above the basal detachment level, which is 10-15 km deep, according to Roca and Guimerà (1992). Most of the available focal mechanisms correspond to normal faults, and are consistent with the recent regional stress field (Herraiz et al. 2000).

The best documented active fault during Pleistocene times is the Concud Fault. This structure has been an object of preliminary paleoseismological characterisation (Simón et al. 2005), morphotectonic analysis (Lafuente et al. 2012), as well as trenching studies (four trenches surveyed at its central and southern sectors, see Figs. 3 and 5; Gutiérrez et al. 2008; Lafuente et al. 2011a, 2014). The results allowed classifying the Concud Fault as a moderately active fault, with recurrent slip since early Late Pleistocene times and maximum estimated moment magnitude (Mw) in the range of 6.4 to 6.8 (Lafuente, 2011; Lafuente et al., 2011a), although no historical destructive earthquake is linked to it. On the other hand, there is a gap of information corresponding to the latest Pleistocene and Holocene, and the hypothesis of additional events not recorded in the previously surveyed trenches has been seriously considered (Lafuente 2011; Lafuente et al. 2014). Searching for new evidence of younger paleoseismic events not yet documented is therefore a critical target.

This paper shows the results of a new trench excavated at the southern sector of the Concud Fault. After comparison with previous results, we are able to refine the paleoseismic succession for Late Pleistocene times and to improve our knowledge of the fault activity pattern. This is then applied to better assess the seismic hazard in Teruel, a city with about 35,000 inhabitants located only 3 km south of the surveyed site.

Also the Teruel Fault, in the neighbourhood of the Concud Fault (Fig. 3), has been object of paleoseismological research. Although evidences of four events occurred between 70.7 ± 5.3 ka and 9.9 ± 0.7 ka BP have been found (Simón et al. in preparation), timing of individual events is not well constrained; the overall Quaternary activity is poorly documented indeed, owing to the extreme scarcity of Quaternary deposits affected by this fault. Therefore, this fault has not provided enough data for being incorporated to seismic hazard analysis made in this paper, so that our present results are based on the Concud Fault as the only seismic source. Trench study in progress in the Teruel Fault and other active fault zones (Sierra Palomera and

Valdecebro, see Figs. 1 and 2) will allow to know more about paleoseismicity of the region, and to achieve more refined seismic hazard assessment in the near future.

2. Geological and structural setting

The central-eastern Iberian Chain includes a number of Neogene-Quaternary extensional basins that represent the onshore deformation of the Valencia Trough (Simón 1989; Roca and Guimerà 1992) and postdate the Alpine compressive structures (Fig. 1). The most recent extensional episode (Late Pliocene-Quaternary) gave rise to the NNW-SSE trending Jiloca Graben and reactivated other grabens (Teruel and Maestrazgo basins) generated in the previous episodes. These structures developed under a regional stress field that has been characterised as a nearly ‘multidirectional’ tension (σ_1 vertical, $\sigma_2 \approx \sigma_3$) with trajectories of the minimum stress σ_3 mainly trending ENE-WSW (Simón 1989; Arlegui et al. 2005).

The Teruel Basin is a half graben with an active eastern boundary made of large, nearly N-S striking faults (Fig. 1), filled with Neogene red clastic alluvial deposits that grade laterally into lacustrine evaporites and carbonates. The age of this infill is well constrained from numerous mammal fossil localities (Godoy et al. 1983a,b; Alcalá et al. 2000), ranging from the early Late Miocene (Vallesian) to the Late Pliocene-earliest Pleistocene (Villafranchian).

The asymmetric Jiloca Graben shows an overall NNW-SSE trend that results from en-echelon, right releasing arrangement of NW-SE striking normal faults, the largest ones being located at the eastern boundary: Calamocha, Sierra Palomera and Concud faults (CaF, PF and CoF in Fig. 1). It is filled with Upper Pliocene to Pleistocene deposits corresponding to alluvial fans, pediments and episodic palustrine environments. In the central sector, these deposits are underlain by lacustrine/palustrine marls of a probable Neogene age (only observed in boreholes; Rubio and Simón 2007).

The Concud Fault is the southernmost fault bounding the Jiloca Graben, and represents the negative inversion of a previous reverse fault (Lafuente 2011; Lafuente et al. 2011a). The trace is 14.2 km long, and shows an overall NW-SE strike that veers towards N-S near its southern tip (Fig. 3); such change in orientation does not involve any structural or seismic segmentation (Lafuente et al. 2011a,b). The fault surface, typically dipping about 70º SW, puts into contact Pleistocene alluvial deposits in the hanging wall with either Triassic and Jurassic units (western and central sectors) or Neogene units belonging to the Teruel Basin (southeastern sector). At its SE tip it approaches the neighbouring Teruel Fault, both showing a right relay arrangement and behaving as independent structures from a geometrical and kinematical point of view (Lafuente et al. 2011b). The kinematic analysis indicates a nearly pure normal movement on the main, NW-SE striking fault segment, while the slip vector on the southern, NNW-SSE striking segment shows a small left-lateral component (striation pitch around 75º S). These kinematical data result in a constant transport direction of the hanging wall towards N 220º E, which indicate that both segments show a complete kinematical compatibility (Lafuente et al. 2011b).

The extensional activity of the Concud Fault, as far as it has been geologically documented, begun by the latest Ruscinian (mid Pliocene), cutting the Upper Miocene-Lower Pliocene infill of the Teruel Basin (Fig. 3). Since that time, sedimentation was interrupted on the footwall, whereas a complete syntectonic sequence belonging to the Upper Pliocene and Quaternary was deposited on the hanging wall (Moissenet 1982; Simón 1983). The Upper Pliocene series includes red, fine-grained alluvial sediments with interbedded lacustrine-palustrine carbonates, and is capped by a pediment cover (*Villafranchian pediment*). The Quaternary deposits are associated to: (i) fluvial terraces of the Guadalaviar and Alfambra rivers, some of them present as well in the footwall: Upper Terrace (T3), Middle Terrace (T2; Middle Pleistocene), Lower Terraces (three sublevels, T1a, T1b, T1c; Late Pleistocene), and Holocene Terrace/flood plain (T0); (ii) short alluvial fans developed from the fault scarp and spreading towards SW, mostly Late Pleistocene in age (Gutiérrez and Peña 1976; Peña 1981; Godoy et al. 1983a,b; Peña et al. 1984; Lafuente 2011).

The average slip rate for the overall extensional history of the Concud Fault can be calculated from the position and age of the youngest pretectonic level, i.e., the top of the Early Pliocene lacustrine deposits at the footwall (Godoy et al. 1983a,b). This level contains fauna belonging to the mammal zone MN 15b (latest Ruscinian; ca. 3.6 Ma; Godoy et al. 1983a,b; Opdyke et al. 1997; Alcalá et al. 2000), and shows a minimum vertical offset of about 240 m (Fig. 4). Considering an average dip of 70º and a pure normal movement, this results in a net displacement of 255 m, which could increase up to 290-300 m if we take into account the probable roll-over geometry at depth. The resulting slip rate is 0.07-0.08 mm/a (Simón et al. 2005; Lafuente 2011; Lafuente et al.

2011a).

3. Methodology

Detailed geological and geomorphological mapping of the southernmost sector of the Concud Fault was carried out to find the suitable place for trenching. This was complemented with topographical and geophysical surveys. Deploying magnetic, electromagnetic and ground-penetrating radar (GPR) methods were use to detect the fault under the soil or superficial regolith.

Classical trench methodology was applied to the selected site: excavating and shoring, cleansing and gridding the most suitable wall, identifying and marking sedimentary boundaries and faults, taking photographs, recording structural and sedimentological information, and sampling relevant materials for OSL dating. Sedimentary units were defined on the basis of lithology, bed geometry, texture, colour and sedimentary structures. In addition, grain size distribution and mineralogical composition of two conspicuous silty levels were determined in order to constrain the correlation of units across the fault (Ezquerro et al. 2014).

After comparing the results in the new trench with those obtained from the previous works, a paleoseismic succession has been reconstructed for the Concud Fault. This provides (within an uncertainty range) the parameters needed for calculating probabilistic seismic hazard based on the concept of characteristic earthquake (Schwartz and Coppersmith 1984). The frequency distribution of recurrence intervals between characteristic earthquakes is the basis of such probabilistic hazard analysis. Several models of statistical distribution have been applied to this problem, the differences arising, quite often, from the source of data (instrumental *vs.* paleoseismic) and the assumed fault recurrence behaviour (Rhoades and van Dissen 2003; McCalpin 2009). Among them, the Gaussian distribution is preferred when the recurrence interval is nearly constant but exhibits some variability (renewal or real time models, Schwartz and Coppersmith 1986), and the data set is not large enough to solidly point to a different distribution (McCalpin 2009); therefore, this is quite often the distribution of choice in paleoseismology. Assuming a probabilistic Gaussian distribution of interseismic periods, the probability of occurrence of a seism equivalent to the characteristic earthquake in a given term (500 years) has been calculated according to the procedure proposed by Schwartz and Coppersmith (1986). The conditional probability is defined as the area under the probability function for the next 500 years, divided by the area under the remaining part of the curve to the right of the present. Required input data for this procedure include the elapsed time, the average recurrence interval and its standard deviation.

4. Trenching at Mataueta site

4.1. Geological and geomorphological setting

The Matraueta trench is located 1 km from the southern tip of the Concud Fault, about 3 km north of Teruel City. It was excavated across an anomalous slope identified within a short Late Pleistocene pediment on the hanging wall block (Fig. 5a). A detailed topographic profile shows an apparent offset of the pediment surface of about 2 m (Fig. 5b). The trench followed the N 085º E direction, parallel to the maximum topographic slope and nearly orthogonal to the main fault trace.

The aforementioned pediment (P1b) links the T1c and T1b terrace sublevels, and its alluvial deposits overlie T1b fluvial deposits (Fig. 5c). Two other terrace levels are present in the hanging wall block in the neighbouring area: T0 and T2. The latter is represented by remains of cemented gravel that crops out either at a higher topographic position close to the fault, or underlying deposits of T1c and T1b (nested terraces).

Below the aforementioned terrace and pediment deposits, two Neogene units (named Páramo 2 and Rojo 3; Late Pliocene to Early Pleistocene in age) locally crop out in the hanging wall block. These units represent the youngest episodes of endorheic sedimentation in the Teruel Basin (Ezquerro et al. 2012). Besides, several older units (Rojo 1 and correlative units, and Páramo 1; Late Miocene) lie horizontally in the footwall of the Concud Fault. A total post-Páramo 2 unit throw of about 230 m can be calculated from the cross-section in the Fig. 4, which has been elaborated from map information, thickness of Neogene units in the neighbouring area and borehole data (Lafuente 2011; Lafuente et al. 2011b, 2014).

The anomalous slope detected in the P1b pediment surface does not coincide with the main trace of the Concud Fault. It runs parallel to the fault strike (NNW-SSE) some 20-25 m west of the main trace. The latter could not be trenched owing to its nearness to the *Vía Verde* touristic road. The possibility that this slope could be associated to a second rupture surface splaying from the main Concud Fault (in the same way as documented in other sectors of the structure; Lafuente 2011; Lafuente et al. 2011a, 2014) was corroborated by the geophysical results: these evidenced a linear anomaly in shallow subsoil levels that was interpreted as a steeply dipping, NNW-SSE striking fault plane cutting Late Pleistocene materials.

4.2. Materials and ages

Five sedimentary units have been distinguished (Units 1 to 5; Fig. 6). These units, excepting the first one, are better and more entirely represented in the hanging wall block. After briefly describing (from bottom to top) the units, we explain how they have been correlated across the fault and we provide OSL ages.

Unit 1: Grey, grain-supported gravels with orange-greyish middle-coarse sandy matrix, laterally and vertically grading into green massive lutites. Gravels are composed by angular to subangular grey calcareous and orange siliceous pebbles with a 6 cm mean diameter, locally reaching 20 cm. There are also thin gravel levels with open framework texture. In the lower part, gravels form tabular or channelled levels, decimetric in thickness, with internal erosion surfaces and horizontal and trough cross stratification. They are locally interbedded with fine sand beds with parallel lamination and massive lutites. The green, massive lutites form irregular levels with some interbedded dm-scale gravel bodies. Lutites include pebbles up to 13 cm in diameter (25 cm in the footwall) and are locally brown, containing white carbonate nodules that indicate pedogenesis. Rounded to subangular black limestone clasts form tabular bodies with crude horizontal stratification (gravel-fine gravel cycles) or channelled bodies with trough cross stratification; clast diametre is lower than 2 cm (5 cm in the footwall) in the tabular bodies and up to 15 cm in the channels.

Unit 2: Grey gravels in channels with internal erosion surfaces, and brown lenticular sand bodies with horizontal and planar cross lamination. The lower part (Subunit 2a) is integrated by grey to orange grain-supported gravels with angular to subangular calcareous, and scarce siliceous clasts with diametres usually ranging from 9 to 16 cm, the biggest ones located on the base of the unit. Matrix is orange medium-size sand. Gravel forms dm-scale channelled bodies or, less commonly, lobate levels. Channels show internal erosive surfaces that separate pebble-granule-sand sequences. The upper part (Subunit 2b) is also made of gravels that, in this case, are grey to brown and intercalate levels of brown middle-coarse sands. Gravels are grain-supported, made of angular to subangular limestone pebbles up to 15 cm in diametre. Matrix is brown-orange medium-coarse sand. Similar sedimentary structures and geometry of sedimentary bodies to those in Subunit 2a are recognized. Sands form dm-scale tabular or lenticular strata, either massive or showing parallel lamination, cross lamination and ripples.

Unit 3: Massive red silts and bad sorted red fine sands with interbedded dm-scale, matrix-supported gravel bodies. Sands, with local calcareous pebbles, constitute cemented tabular levels up to 0.2 m thick with horizontal lamination. Gravels consist of calcareous rounded pebbles, with mean diametre of 6-8 cm, although subangular pebbles up to 15 cm are occasionally scattered through the deposit. Gravel bodies are tabular with local channelled or slightly erosive bases. One of the tabular bodies allows separating this unit into two main parts (Fig. 6): Subunit 3a, with varying thickness from 30 to 90 cm due to erosive truncation on top, and Subunit 3b, with a more homogeneous thickness, about 80-90 cm.

Unit 4: Massive red to orange silty lutites with an erosive gravel body at the bottom. The whole unit shows pedogenic evidence, displaying scattered carbonate nodules. Lutites include local angular pebbles up to 12 cm in diameter. Gravels consist of grey, matrix-supported gravels with subangular, homometric pebbles up to 15 cm in diameter, and reddish silty matrix that locally becomes greyish and microconglomeratic. They form a strongly channelled body, 0.3-0.5 m thick, which locally erodes the underlying units; moreover it contains internal erosive surfaces and associated pebble lags.

Unit 5: Brown, poorly compacted massive lutites with scattered clasts and carbonate nodules; root bioturbation is common. It represents a very thin colluvium or regolith that has been reworked due to agricultural labours.

The described features allow interpreting these materials as deposited in a proximal alluvial system. Units 1 and 2 represented deposition in the active sector that was dominated by gravel channels and bars. Units 3 and 4 are more typical of the floodplain zone where fine terrigenous facies predominated with coarser facies only reaching this area during higher-energy flooding stages. The observed rapid lateral facies changes are typical of pediment deposits, as they are dominated by discontinuous sedimentation and shifting channels. Such facies changes and variations in thickness add some uncertainties in the correlation of units 1 to 4 between both fault blocks. Aiming to support the proposed correlation (and to make optimal paleoseismological estimations), eleven samples were taken from two conspicuous lutite levels (top of Unit 1 and top of Unit 3) present at both fault blocks. Grain-size and mineralogical results (Ezquerro et al. 2014) allowed confirming the initial correlation (Fig. 6). This correlation suggests that, as expected, erosive processes were dominant at the footwall block, so units were preserved only partially.

OSL dating of units has been performed from ten samples (Table 1; see location in Fig. 6). Unit 5 has not been dated because its continuous removing by farming works makes it unsuitable. OSL ages indicate that the record in the hanging wall block of the fault has been relatively continuous and comprises from ca. 21.3 ka (top of Unit 1) to ca. 12.8 ka BP (top of Unit 4). Sedimentary levels in the fault zone and in the footwall block usually provide younger OSL ages than the corresponding ones in the hanging wall block (e.g., units 1, 2 and 3). The position of these samples in the vicinity of erosive surfaces suggests rejuvenation processes, as discussed in detail by Ezquerro et al. (2014).

4.3. Fault geometry and kinematics

The main surveyed fault zone, with an overall trend N 165º E and dip 67º W, is made of several fault surfaces (Fig. 7). Unfortunately, no striation was observed on it, so that the precise slip vector is unknown. Nevertheless, considering the overall transport direction of the hanging wall towards N 220º E (Lafuente et al. 2011b), a virtual slip vector with a rake of 77º S could be inferred.

The hanging wall block shows further deformation (Figs. 6, 7): (i) a single antithetic fault oriented 160/65º E and located at a distance of about 10 m from the main fault zone; (ii) a gentle roll-over affecting units 1, 2 and 3a, attaining a maximum dip of 8º E.

4.4. Interpretation of events

The detailed study of sedimentary units, deformation and relationship with faults allows interpreting three seismic events, with a ‘creep-like’ stage following the first event (Table 2). The determination of coseismic displacements is based on objective measurement of the vertical separation (throw) of discrete markers on the trench walls. The net slip values were then calculated by considering the overall dip of the fault zone

(70º W) and the virtual rake of the transport direction (77º S). This resulted in a correction factor of 1.09 (net slip = throw / (sin 70º · sin 77º). As an auxiliary tool, retrodeformational analysis (Fig. 8) allowed us to construct the whole interpretation and to refine coseismic displacement values.

- **Event X_M.** Evidenced by the rupture and displacement of Subunit 2a by fault Fα, subsequently covered by Subunit 2b (Fig. 6, cells 17a,b). Subunit 2a is only present in the downthrown block, although its sedimentological features and geometrical relationship with the Fα surface suggest that it was deposited as well on the upthrown block, then completely removed due to erosion by channels at the base of Subunit 2b (Fig. 8a,b,c). Such hypothesised erosion would involve that the apparent measured throw T_x = 1.2 m (Fig. 9) is just a minimum value. The event age is bracketed between 21.3 ± 1.5 ka (Unit 1) and 21.0 ± 1.4 ka (Subunit 2b), prompting a most probable event age of 21 ka.

- **'Creep-like' stage.** The variable thickness and internal structure of Unit 3 (Fig. 6) suggests a progressive displacement along fault Fβ, mainly coeval with sedimentation of Subunit 3a. Such deformation could occur as either a creep stage or, alternatively, a succession of minor events not identifiable as characteristic earthquakes (recognizing true aseismic creep in trenches is a highly complex task, submitted to great uncertainties). Probably, it also involved propagation of Fα into Subunit 2b, which would have produced the sharp (although of limited amplitude) drag fold associated to its upper, overhanging segment. Displacement along Fβ would have generated a hanging wall roll-over anticline on top of Subunit 2b, thus creating an accommodation space that was contemporary filled by Subunit 3a (Fig. 8d). Subsidence associated to this episode was comprised between 1.1 m (minimum throw on Fβ) and 1.4 m (adding the amplitude of the drag fold on Fα). Nevertheless, since it seems related to roll-over accommodation, i.e., back-tilting of the downthrown block, it does not represent its true tectonic displacement (McCalpin, 1996, p. 101). Subunit 3b shows more constant thickness, and is locally separated from 3a by a gentle unconformity (see cell 10d in Fig. 6). Therefore, it seems to have been deposited nearly horizontal, once the roll-over accommodation space had been almost completely filled (Fig. 8d,e). Thus, it can be inferred that the 'creep' stage started soon after 21.0 ± 1.3 ka (top of Subunit 2b) and finished long before 19.2 ± 1.2 ka (upper part of Subunit 3b).

- **Event Y_M.** Evidenced by displacement (with associated gentle drag folding) of Subunit 3b along fault Fβ, then buried beneath the base of Unit 4 (Figs. 6 and 8f,g, cell 18b). The apparent measured throw (T_y, including drag fold) can be estimated in the range of 0.7 to 0.9 m (Fig. 9). Pre- and postdating ages are 19.2 ± 1.2 ka and 16.4 ± 1.0 ka, respectively, corresponding to samples collected at similar distances from the erosive base of Unit 4. Therefore, we consider the middle of this time range (ca. 18 ka BP) as the most probable age for this event.

- **Event Z_M**. Evidenced by displacement of Unit 4 along faults Fγ (a new rupture surface belonging to the main fault zone, cells 19f,g) and Fδ (an antithetic fault newly created during this event, cell 3e: no evidence of activity during sedimentation of previous units was found) (Figs. 6, 8h). The ensemble was then strongly eroded and covered by the subactual colluvium (Unit 5) (Fig. 8i). The throw at the base of Unit 4 has been calculated with uncertainties derived from (i) the uneven geometry of this marker, and (ii) its removing in the footwall within a distance of seven metres from the main fault, which compel us to extrapolate its trace in order to measure the separation on the trench log. Using a smoothed envelope of this geologic surface in order to minimize such uncertainties, the apparent throw T_z has been measured as around 2.6 m (Fig. 9). The event age is predated by 12.8 ± 0.7 ka (upper part of Unit 4); unfortunately, no absolute postdating age is available for Unit 5.

The observed throws assigned to these three events (T_x, T_y, T_z) plus the 'creep' component broadly coeval of Subunit 3a totalize up to 6.1 m (Fig. 9), equalling the total offset exhibited by the silty level on top of Unit 1, a sedimentary marker carefully correlated between both fault blocks (Ezquerro et al., 2014). Nevertheless, they do not represent their real tectonic throws. Both roll-over deformation (subsidence up to 1.4 m) and slip along the antithetic fault (Tδ = 0.4 m, ascribed to event Z_M) should be interpreted as products of gravitational accommodation of the hanging-wall block. Therefore, in order to evaluate and balance the real coseismic slip values, the observed throws should be diminished by the throws associated to both structures, as stated by McCalpin (1996, p. 103) and Caputo et al. (2008). This correction can be achieved by extrapolating sedimentary markers over the graben, so defining virtual tip points at the hanging-wall (open circle, square and triangle in Fig. 9). In this way, the real tectonic throw of event Z_M can be directly measured by extrapolating the base of Unit 4: $TT_Z = TT_4 = 2.2$ m (Fig. 9). This results in a net coseismic slip of $2.2 \cdot 1.09 = 2.4$ m. In the same way, real tectonic throws can be measured for the base of Unit 3 (TT_3 = 2.9 m) and the base of Unit 2 (TT_2 = 4.3 m), the last one being directly based upon the correlation of the silt level on top of Unit 1 (Ezquerro et al., 2014). Hence, we calculate the real coseismic throws associated to events Y_M and X_M: $TT_Y = TT_3 – TT_4$ = 0.7 m (net coseismic slip = 0.8 m); $TT_X = TT_2 – TT_3$ = 1.4 m (net coseismic slip = 1.5 m), respectively (Table 2).

5. Integrating previous and new results: paleoseismic history of the Concud Fault

So far, the paleoseismic history of the Concud Fault has been fairly known through the paleoseismological analysis of four trenches: Los Baños, Masada Cociero, El Hocino 1, and El Hocino 2 (Lafuente 2011; Lafuente et al. 2010, 2011a, 2014; Simón et al. 2012). These yielded nine events for the time lapse between ca. 74 and 15 ka BP, four of which were correlated between different trenches (events 1 to 8, and 10 in Fig. 10).

Based on the new information from the presented trench combined with the previous results, the paleoseismic succession was further enhanced and extended. Event X_M identified in the Mataueta trench, with the most probable age of 21 ka BP, corresponds well with event Z_{H2} of El Hocino (Lafuente et al. 2014) (Fig. 10). Event Y_M, with the most probable age around 18 ka, presents some uncertainty. There are two possible interpretations in relation to the previously established paleoseismic succession. The first one is that this event corresponds to Z_{MC} at Masada Cociero trench, robustly dated to around 15 ka BP. The second one is that Y_M is distinct from Z_{MC}, so that Y_M represents an additional event between 21 ka and 15 ka. The second hypothesis strongly diminishes the interseismic period for the latest Pleistocene earthquakes. On the other hand, the first one requires forcing the whole error bar of the postdating age (16.4 ± 1.0 ka), involving that the age of around 15 ka for the event Y_M of Mataueta trench is more accurate than the 18 ka initially considered; furthermore, it involves that both fault branches (Mataueta and Masada Cociero) would have been activated simultaneously, so that the total net slip on the root fault would roughly equal the sum of both observed displacements (2.2 m + 0.8 m = 3.0 m). This is a value beyond both the expected and the observed range of coseismic slip on the Concud Fault (Lafuente et al. 2011a, 2014). Therefore, we consider the second hypothesis ($Y_M \neq Z_{MC}$) as more likely. Concerning the latest event recorded at Mataueta site (Z_M), we know that it is younger than 12.8 ± 0.7 ka, so it also represents a new, not previously defined paleoearthquake. Unfortunately, no further time constrain does exist owing to the lack of postdating age in the surveyed trench. Therefore, we can only argue that it occurred before deposition of the non-deformed Holocene terrace, with an OSL age of 3.4 ± 0.7 ka (Lafuente 2011; Lafuente et al. 2014).

In total, eleven events that have occurred since 74 ka BP were reconstructed (Figs. 10, 11). Two of them had not been detected in the previous paleoseismological studies. The total cumulative displacement is 20.5 m with an average coseismic slip of 1.9 m. Unfortunately we have not been able to establish neither the age of the last recorded event nor whether it represents the last event attributable to the Concud Fault activity. This generates some uncertainty in seismic hazard assessment, as addressed below.

The average slip rate of the fault exposed at the Mataueta trench can be obtained, as the first approach, from the net tectonic throw (4.3 m) measured from the oldest marker surveyed in the trench (base of Unit 2a, dated close to 21.3 ± 1.5 ka BP). After applying the correction factor (1.09), the resulting net tectonic slip is 4.7 m, and the net slip rate for the whole period is 0.20 ± 0.02 mm/a. If the total slip history since ca. 21 ka BP is considered for this sector of the Concud Fault, we should (i) add the coseismic slip measured at Masada Cociero (event Z_{MC}, up to 2.2 m; Lafuente et al. 2014), and (ii) take into account the age range estimated for the youngest recorded event (12.8 ± 0.7 ka to 3.4 ± 0.7 ka; absolute range: 13.5 ka to 2.7 ka; mean = 8.1 ka). In this way, a slip rate ranging from 0.30 to 0.72 mm/a (mean = 0.42 mm/a) is derived for the latest recorded paleoseismic history (Fig. 11).

The slip rate during this period is higher than the average rate for the whole paleoseismic succession recorded at the Concud Fault for Late Pleistocene times (0.29 mm/a). Indeed, the overall paleoseismic pattern is characterised by alternating periods of fast slip (74.5 to 60 ka BP, 0.53 mm/a; 21 to ca. 8 ka BP, 0.42 mm/a) and slow slip (60 to 21 ka BP, 0.13 mm/a) (Fig. 11).

6. Probabilistic seismic hazard analysis based on the characteristic earthquake of the Concud Fault

In seismic hazard assessment, hazard models and probability of occurrence of a given seism are obtained via the application of a recurrence model to a set of geological parameters that include slip rate, recurrence interval, displacement/event, fault geometry, and elapsed time from the last paleoseismic event (McCalpin, 2009).

Previous paleoseismological studies had demonstrated that the Concud Fault has been active since the Middle Pliocene, with slip rates ranging from 0.08 to 0.33 mm/a, and potential to generate earthquakes up to M ≈ 6.8 (Simón et al. 2005, 2012; Lafuente 2011; Lafuente et al. 2007, 2008a,b, 2010, 2011a, 2012, 2014). The total palaeoseismic succession reconstructed after those studies, and significantly expanded in the present work, includes eleven seismic events occurred since 74 ka, with a recurrence interval constrained between 7.1 ± 3.5 and 8.0 ± 3.3 ka and average coseismic displacement of 1.9 m. This succession represents a consistent activity pattern from which seismic hazard analysis based on the characteristic earthquake can be made.

The seismic potential of the Concud Fault, i.e. the moment magnitude (Mw) that can be assigned to such characteristic earthquake is in the range of 6.4 to 6.8 (Lafuente 2011; Lafuente et al. 2011a). This estimation is based on its trace length (14.2 km) and its lack of segmentation, and was made using empirical relations proposed by Wells and Coppersmith (1994), Stirling et al. (2002) and Pavlides and Caputo (2004). Ezquerro et al. (2015, Appendix 1) introduced the parameters of the most probable scenario for the characteristic earthquake (rupture of the total length up to a 14 km-deep detachment level, maximum coseismic slip 1.9 m) in the original equation that defines Mw (Hanks and Kanamori, 1979), obtaining a range of Mw from 6.5 to 6.6.

The uncertainty about the age of the youngest event compel us to consider a number of distinct hypotheses on the *elapsed time* in order to approach the probabilistic seismic hazard: (h1) 13.5 ka, maximum value; (h2) 8 ka, arbitrary middle value; (h3) 2.7 ka, minimum value. These hypotheses give rise to three values for the average interseismic period (between 7.1 ± 3.5 and 8.0 ± 3.3 ka), as compiled in Table 3.

Assuming a probabilistic normal distribution of interseismic periods, and considering each of the three aforementioned hypotheses for the age of the youngest event, the probability of occurrence of a seism equivalent to the characteristic earthquake in a given term (500 years) has been calculated (Table 3) according to the procedure proposed by Schwartz and Coppersmith (1986). It can be seen how the elapsed time is a critical parameter, since it makes the probability to vary between 2.3% and 26.1%.

7. Discussion

7.1. On the temporal variation of slip rates

The average slip rate of the Concud Fault during Late Pliocene–Pleistocene times approaches those of other major faults in the central–eastern Iberian Chain: Sierra Palomera, Calamocha, Sierra del Pobo, Teruel and Maestrat faults (all of them within the range of 0.06-0.15 mm/a; Simón et al. 2012). Nevertheless, slip rates at many of these faults tend to decay with time (particularly, at the eastern Maestrat graben system: 0.04-0.18 mm/a for the last 3.6 to 5.0 Ma vs. 0.02-0.05 mm/a for the last 1.9 to 2.6 Ma; Simón et al. 2012), while slip rate at the Concud Fault tends to increase: 0.29 mm/a in average during Late Pleistocene times (this work) vs. 0.07-0.08 mm/a for the last 3.6 Ma (Lafuente 2011; Lafuente et al. 2011a). The only structure in which a comparable slip rate has been documented is the near–shore Torreblanca Fault (0.26-0.30 mm/a for the last 253.3 ± 18.0 ka; Simón et al. 2013).

Its increasing slip rate during Late Pleistocene makes the Concud Fault as active as some normal faults of the Betic Chains, e.g. Granada Fault (0.03-0.38 mm/a; Sanz de Galdeano et al. 2003) or Baza Fault (0.12-0.33 mm/a; Alfaro et al. 2008; García-Tortosa et al. 2008). This seems to be unusual if we take into account its regional setting (gentle tectonic deformation, low instrumental seismicity). Nevertheless, it could be explained if the total crustal deformation of the central–eastern Iberian Chain, formerly distributed among a number of large faults, was progressively concentrated into a few ones during Pleistocene times, as documented in other regions (e.g. central Apennines, Italy, since 0.9 Ma; Roberts et al. 2002). The Concud Fault could finally accommodate an important fraction of the total crustal extension at this sector of the Iberian Chain (Lafuente et al. 2014).

Such hypothesised tendency would obviously increase seismic hazard in the region surrounding the Concud Fault. The reconstructed paleoseismic succession (11 seismic events since 74 ka, with a recurrence interval constrained between 7.1 ± 3.5 and 8.0 ± 3.3 ka) represents a fairly complete record that draws a consistent activity pattern on which our hazard analysis is based. Nonetheless, we should be aware that uncertainties related to (i) temporal variation of slip rate and (ii) the poorly constrained age of the last recorded event (between 13.5 and 3.4 ± 0.7 ka BP) still remain.

Temporal variation of slip rate, already pointed out in the previous studies (Lafuente et al. 2011a, 2014), is now reinforced on the basis of a more complete paleoseismic succession. The results of paleoseismological analysis of the Mataueta trench suggest the notion of a roughly cyclical activity of the fault during Late Pleistocene times. Three periods can be distinguished, two of them characterised by rapid slip (74.5 to 60 ka BP, 0.53 mm/a; 21 to ca. 8 ka BP, 0.42 mm/a), and separated by a period of slow slip (60 to 21 ka BP, 0.13 mm/a). The slip history of the Concud Fault (Fig. 11) suggests that its present-day tendency is represented by a high-activity period, with slip rate of 0.42 mm/a and average recurrence period of ca. 4.3 ka. Significantly higher seismic hazard values would be obtained by using these quantities in our probability calculations.

7.2. On the characteristic earthquake model and the uncertainties of our seismic hazard analysis

The probabilistic hazard analysis made in the present work is based on the characteristic earthquake defined from paleoseismological study of the Concud Fault. The characteristic earthquake model assumes that most strain is released in large earthquakes that fall within a narrow window of magnitude range (Schwartz and Coppersmith 1984). It also implicitly assumes that the ruptures are limited to persistent segments, the displacement per event at a point is nearly constant, and the slip rate along strike is variable. Given that the type and strength of fault zone materials as well as the regional stress regime may remain relatively constant, it would be expectable that the characteristic earthquakes were generally of uniform size, as well.

Obviously, other approaches are possible, based on alternative models of earthquake behaviour. Reid's Perfectly Periodic model (Reid 1910) postulates that earthquakes occur whenever stress builds up to a given level, and the stress drop and magnitude of each earthquake are identical. If stress build up through time is constant then the earthquakes become perfectly periodic. Shimazaki and Nakata (1980) expanded this model into the Time-Predictable model, where quakes occur at constant critical stress level but the stress drop and magnitude vary (thus the time of the next earthquake can be predicted from the slip in the previous earthquake), and the Slip-Predictable model that makes the contrary assertion: earthquakes always fall back to a given stress level, and thus slip in the next earthquake can be predicted from the time since the previous earthquake. As during earthquakes slip usually varies along fault strike, the need to incorporate this variation along the fault trace arose, and Variable and Uniform Slip models (see McCalpin 2009 for a review) were born**.** Each of them could give rise to diverse procedures of hazard analysis and different results.

Variable slip models estipulate that slip rate along fault strike is constant, but that displacement per event at a point, and thus the earthquake size, is variable. In our case, we can discard the variable slip models in benefit of the uniform slip model because the observed displacements in our paleoseismic succession a re rather constant for a given site (i.e., the coefficient of variation, standard deviation/mean, at los Baños site is 0.38 so as the mean slip is ca. 2 m, 67% of observed slip fall between 1.2 and 2.7 m, Lafuente et al. 2011a). Among this family of models most distinctions depend on the presence of persistent segments, which in the case of the Concud Fault do not exist. Thus, the Characteristic Earthquake model (that belongs to the uniform slip family) could be of application, as its main assumptions agree with the observed behaviour: paleoseismic observations of large displacements at trench sites, with very little evidence of smaller displacement events; near constant displacement per event in each point of the fault, but variable along its trace; and, as a result, decrease on the structural relief at the boundaries of our single-segmented fault.

Though this is probably the most favoured model for paleoseismologists (Liu et al. 2004), some authors have described paleoearthquake faulting chronologies that are “noncharacteristic” (Roberts 1996; Maruyama et al. 2007), which suggests that paleoseismic surveys are able to allow to discriminate between behaviour models. Indeed, in the Teruel region we have found paleoseismic successions that include displacements significantly smaller than the mean slip at a particular site, thus deserving to be considered “noncharacteristic” events (event of 0.1 m slip *versus* mean slip of about 0.5 m at a trench in the Teruel Fault, Simon et al., in preparation). As a note of interest, such value of 0.1 m could very well represent, at least in coarse clastic sediments, a resolution threshold for event recognition under which it is not possible to identify individual events. An ensemble of discrete events whose respective displacements fall below this ‘paleoseismological pixel size’ could very likely be the foundation of what we have called elsewhere ‘creep-like’ stage.

There is not a general agreement on whether the characteristic earthquake model could successfully represent how faults in low strain regions behave. The wide gap that usually exists between the limited historical record and the long recurrence periods of such moderately active faults feeds the doubts about it. In the case of the Concud Fault, although such time gap indeed exists, a high coherency has been found between both extremes. The parameters of the characteristic earthquake of the Concud Fault (Mw ≈ 6.5-6.6; recurrence period = 7.3 ± 2.7 ka) fit precisely the magnitude-frequency pattern obtained from the historical and instrumental seismicity of the Teruel and Jiloca grabens (Fig. 12). In our view, the whole area behaves as a homogeneous seismic zone, with a common energy dissipation pattern through seismic shakes. Part of the energy is released by multiple slip on small faults, while only scarcely the rupture of a major fault as Concud leads to the characteristic earthquake. This seismotectonic zone may be the proper domain where to interpolate between historic-instrumental and paleoseismic records. This exercise of interpolation allowed us to estimate of the maximum expectable seism within a 500-year period: M = 5.33 ± 0,3 (Fig. 12; Simón et al. 2014).

With respect to the elapsed time, which is of capital importance as previously shown in probabilistic modelling, it may prove to be one of the most difficult parameters to ascertain. Concerning the age of the last paleoseismic event, given that the paleoseismic history of the fault between 13.5 ka and 2.7 ka BP could not be reconstructed: (i) we are uncertain about the age of Z_M within this time span, and (ii) we are not able to ensure that this actually represents the last one at the Concud Fault. Additional, relevant information can be obtained from the only deformed marker exposed on both fault blocks in this area. Such marker is represented by two remains of the higher sublevel of the Lower Terrace (T1c) present on both fault blocks, some 0.5 km SSE of Masada Cociero (Fig. 5). A post-T1c fault throw of about 8 m can be inferred from the height difference of both remains of this terrace level (943-944.5 m.a.s.l. in the footwall block; 935.5-936.5 m.a.s.l. in the hanging wall block). The terrace remain within the hanging wall block is now buried below the A-23 highway, but we could obtain those precise height values from the previous detailed topographic map (Ministerio de Fomento 1999, unpublished). After applying the correction factor imposed by the obliqueness of the transport direction, the estimated net tectonic slip is 8.7 m. T1c deposits within the footwall block have been dated to 22.0 ± 1.6 ka BP (Table 1) in a neighbouring outcrop some tens of metres east of the area mapped in Fig. 5. They should therefore undergo displacement due to four younger events (X_M, Y_M, Z_{MC}, and Z_M), which, according to our trench studies, accumulated a total displacement of 6.9 m. The difference between both values (8.7 m – 6.9 m = 1.8 m) is close to the average coseismic slip inferred from the overall paleoseismic succession (1.9 m), so it is consistent with the hypothesis of an additional, still not identified paleoseismic event. Further research is therefore required in order to refine seismic hazard assessment in the area.

7.3. On the seismic hazard assessment in Teruel city

The probabilistic hazard analysis made in the present work, based on the characteristic earthquake defined from paleoseismological study of the Concud Fault, strongly differs from that established by Spanish regulations for earthquake-resistant building up to the present day (*Norma de Construcción Sismorresistente*, NCSR-02, Ministerio de Fomento 2002). Those ones only consider seismic hazard based upon historic and instrumental seismicity. The city of Teruel has been out the scope of such regulations, since the local calculated seismic acceleration for a recurrence period of 500 years was under the applicable threshold of 0.04 g.

At present, a methodological change is in progress, so that data on seismic sources (García Mayordomo et al., 2012) are being progressively introduced into seismic hazard assessment. As a result, hazard maps published by IGN (Spanish Geographical Survey, the institution entrusted with the task of defining official seismic hazard in Spain) have been significantly modified (Martínez Solares et al. 2013), although such changes have not yet been translated into public earthquake-resistant building regulations.

A recent case pertinently illustrates how the paleoseismological parameters defined here for the Concud Fault can be successfully applied to seismic hazard assessment. In 2012 the Aragón regional government presented the new project for a public hospital of Teruel, at a site 400 m far from the Concud Fault. By strict application of the current regulations, it was exempted of using the seismic-safe building practices, as stated above. Our team was tasked by the Aragón government to carry out a seismic hazard analysis based upon our knowledge of the seismic potential of the Concud Fault. In our conclusions we presented an estimate of the maximum expectable seism within a 500-year period: M = 5.33 ± 0.3. Empirical correlations from this value provided a potential intensity at the hospital site of I ≥ VII, and a peak ground acceleration $a_p = 0.105g$ (Simón et al., 2014). At the light of our report, and because of the discrepancy with the current legal situation, the Aragón government then requested IGN and Instituto Geológico y Minero de España (IGME, the geological survey of Spain) for additional independent reports. Both institutions concluded, in a similar vein, that a seismic–safe building procedure was in order. In particular, IGN modified the seismic acceleration attributed to Teruel city, and calculated a design ground acceleration (ground acceleration that derives from the basic PGA and the geotechnical conditions in site, and determines appropriated building procedures in the NCSR-02 regulation) of 0.092g (Cabañas and Martínez Solares 2013). Finally, the Aragón government decided to adapt the building project to the newly proposed seismic parameters.

8. Conclusions

Results at the presented Mataueta trench have significantly extended the paleoseismological record of the Concud Fault. Three successive events have been interpreted at minor faults splaying at a short distance from the main fault. Event X_M, with the most probable age of 21 ka BP, is correlated with event Z_{H2} previously characterised at El Hocino site (Lafuente et al. 2014). Events Y_M (ca. 18 ka) and Z_M (younger than 12.8 ± 0.7 ka, older than 3.4 ± 0.7 ka) were not identified in previous studies. Unfortunately, owing to the lack of continuous sedimentary record during Holocene times, the age of the youngest event cannot be better constrained. Neither we are confident on whether Z_M actually represents the last event in the Concud Fault; independent constraints from the offset of a neighbouring fluvial terrace support the hypothesis of an additional, still not identified paleoseismic event indeed.

After incorporating these results, the total paleoseismic succession reconstructed for the Concud Fault consists of eleven events occurred since 74.5 ka BP to the present day (Fig. 10), with an average interseismic period constrained between 7.1 ± 3.5 and 8.0 ± 3.3 ka. They totalise a net cumulative slip of about 20.5 m, with an average coseismic slip of 1.9 m. The average slip rate for the total recorded period is 0.29 mm/a, but the displacement pattern is characterised by alternating periods of fast slip (74.5 to 60 ka BP, 0.53 mm/a; 21 to ca. 8 ka BP, 0.42 mm/a) and periods of slow slip (60 to 21 ka BP, 0.13 mm/a).

This paleoseismic succession, together with the potential magnitude previously attributed to the characteristic earthquake at the Concud Fault (M ≈ 6.5-6.6; Lafuente et al. 2014), has served as input for probabilistic seismic hazard analysis. Owing to the uncertainty about the age of the youngest event, three distinct hypotheses on the *elapsed time* have been considered (13.5 ka, 8 ka, and 2.7 ka). The estimated probability of occurrence of the characteristic earthquake in a 500-years term is 2.3%, 19.3%, and 26.1%, respectively.

In spite of their uncertainties, the paleoseismological parameters defined for the Concud Fault (main potential seismic source in the area) have provided critical inputs for improving seismic hazard assessment in Teruel city.

Acknowledgements

The research has been financed by project CGL2012-35662 of Spanish Ministerio de Economía y Competitividad-FEDER, as well as by the Aragón regional government (E27, Geotransfer research group). L. Ezquerro benefited from a FPI grant (BES-2010-031339) of Spanish Ministerio de Economía y Competitividad. We thank the Laboratorio de Datación y Radioquímica de la Universidad Autónoma de Madrid for OSL dating. Valuable comments by P. Stepancikova and an anonymous reviewer greatly contributed to improve the manuscript.

References

Alcalá L, Alonso-Zarza AM, Álvarez MA, Azanza B, Calvo JP, Cañaveras JC, van Dam JA, Garcés M, Krijgsman W, van der Meulen AJ, Morales J, Peláez P, Pérez-González A, Sánchez S, Sancho R, Sanz E (2000) El registro sedimentario y faunístico de las cuencas de Calatayud-Daroca y Teruel. Evolución paleoambiental y paleoclimática durante el Neógeno. Revista de la Sociedad Geológica de España 13: 323-343.

Alfaro P, Delgado J, Sanz de Galdeano C, Galindo-Zaldívar J, García-Tortosa FJ, López-Garrido AC, López-Casado C, Marín C, Gil A, Borque MJ (2008) The Baza Fault: a major active extensional fault in the Central Betic Cordillera (South Spain). International Journal of Earth Sciences 97: 1353-1365.

Allen CR (1986) Seismological and paleoseismological techniques of research in active tectonics. In: Wallace RE (ed) Active Tectonics. Studies in Geophysics, National Academy Press, Washington, pp 148-154.

Arlegui LE, Simón JL, Lisle RJ, Orife T (2005) Late Pliocene-Pleistocene stress field in the Teruel and Jiloca grabens (eastern Spain): contribution of a new method of stress inversion. Journal of Structural Geology 27: 693-705.

Cabañas L, Martínez Solares JM (2013) La peligrosidad sísmica en el emplazamiento del nuevo Hospital General de Teruel. Informe del IGN al Gobierno de Aragón. Unpublished.

Caputo R, Pavlides S, Mucciarelli M (2008) Magnitude distribution of linear morphogenic earthquakes in the Mediterranean Region: insights from palaeoseismological and historical data. Geophysical Journal International 174: 930-940. doi: 10.1111/j.1365-246X.2008.03834.x.

Ezquerro L, Lafuente P, Pesquero MD, Alcalá L, Arlegui LE, Liesa CL, Luque L, Rodríguez-Pascua MA, Simón JL (2012) Una cubeta endorreica residual del Pleistoceno inferior en la zona de relevo entre las fallas neógenas de Concud y Teruel, Cordillera Ibérica: implicaciones paleogeográficas. Revista de la Sociedad Geológica de España 25: 157-175.

Ezquerro L, Liesa CL, Simón JL, Arlegui L, Luzón A, Lafuente P. (2014) Correlation of sedimentary units from grain-size and mineralogic analyses as a tool for constraining trench interpretation in paleoseismology. International Journal of Earth Sciences 103: 2337-2333.

Ezquerro L, Moretti M, Liesa CL, Luzón A, Simón JL (2015) Seismites from a well core of palustrine deposits as a tool for reconstructing the palaeoseismic history of a fault. Tectonophysics (in press).

García-Mayordomo J, Insua-Arévalo JM, Martínez-Díaz JJ, Jiménez-Díaz A, Martín-Banda R, Martín-Alfageme S, Álvarez-Gómez JA, Rodríguez-Peces M, Pérez-López R, Rodríguez-Pascua MA, Masana E, Perea H, Martín-González F, Giner-Robles J, Nemser ES, Cabral J, QAFI compilers (2012) The Quaternary Active Faults Database of Iberia (QAFI v.2.0). Journal of Iberian Geology 38 (1): 285-302.

García-Tortosa FJ, Sanz de Galdeano C, Sánchez-Gómez M, Alfaro P (2008) Geomorphologic evidence of the active Baza Fault (Betic Cordillera, South Spain). Geomorphology 97: 374–391.

Godoy A, Ramírez JI, Olivé A, Moissenet E, Aznar JM, Aragonés E, Aguilar MJ, Ramírez del Pozo J, Leal MC, Jerez-Mir L, Adrover R, Goy A, Comas MJ, Alberdi MT, Giner J, Gutiérrez-Elorza M, Portero JM, Gabaldón V (1983a) Mapa Geológico de España 1:50.000, hoja nº 567 (Teruel) y memoria. IGME, Madrid.

Godoy A, Olivé A, Moissenet E (1983b) Mapa Geológico de España 1:50.000, hoja nº 542 (Alfambra) y memoria. IGME, Madrid.

Gutiérrez M, Peña JL (1976) Glacis y terrazas en el curso medio del río Alfambra (provincia de Teruel). Boletín Geológico y Minero 87: 561-570.

Gutiérrez F, Gutiérrez M, Gracia FJ, McCalpin JP, Lucha P, Guerrero J (2008) Plio-Quaternary extensional seismotectonics and drainage network development in the central sector of the Iberian Range (NE Spain). Geomorphology 102: 21-42.

Hanks TC, Kanamori H (1979) A moment magnitude scale. Journal of Geophysical Research 84: 2348-2350.

Herraiz M, De Vicente G, Lindo-Ñaupari R, Giner J, Simón JL, González-Casado JM, Vadillo O, Rodríguez-Pascua MA, Cicuéndez JI, Casas A, Cabañas L, Rincón P, Cortés AL, Ramírez M, Lucini M (2000) The recent (upper Miocene to Quaternary) and present tectonic stress distributions in the Iberian Peninsula. Tectonics 19: 762-786.

IGN (2010) Servicio de Información Sísmica del Instituto Geográfico Nacional. http://www.ign.es/ign/es/IGN/SisCatalogo.jsp. Accessed December 2010.

Lafuente P (2011) Tectónica activa y paleosismicidad de la falla de Concud (Cordillera Ibérica central). PhD Thesis, Universidad de Zaragoza.

Lafuente P, Simón JL, Rodríguez-Pascua MA, Arlegui LE, Liesa CL (2007) Aproximación al comportamiento paleosísmico de la falla de Concud (Teruel, Cordillera Ibérica). Actas III Congreso Nacional de Ingeniería Sísmica, Girona, Asociación Española de Ingeniería Sísmica, pp 211-223.

Lafuente P, Lamelas T, Soriano MA (2008a) Caracterización morfotectónica de la actividad de la falla de Concud (Cordillera Ibérica, Teruel). Geo-Temas 10: 1027-1030.

Lafuente P, Rodríguez-Pascua MA, Simón JL, Arlegui LE, Liesa CL (2008b) Sismitas en depósitos pliocenos y pleistocenos de la fosa de Teruel. Revista de la Sociedad Geológica de España 21: 133-149.

Lafuente P, Arlegui LE, Liesa CL, Simón JL (2010) Nuevo estudio paleosismológico en el sector central de la falla de Concud (fosa del Jiloca, Teruel): resultados preliminares. In: Insua JM, Martín-González F (eds) Contribución de la Geología al Análisis de la Peligrosidad Sísmica, Sigüenza (Guadalajara, España), pp 67-70.

Lafuente P, Arlegui LE, Liesa CL, Simón JL (2011a) Paleoseismological analysis of an intraplate extensional structure: the Concud fault (Iberian Chain, Spain). International Journal of Earth Science 100: 1713-1732. doi: 10.1007/s00531-010-0542-1.

Lafuente P, Arlegui LE, Casado I, Ezquerro L, Liesa CL, Pueyo Ó, Simón JL (2011b) Geometría y cinemática de la zona de relevo entre las fallas neógeno-cuaternarias de Concud y Teruel (Cordillera Ibérica). Revista de la Sociedad Geológica de España 24: 117-132.

Lafuente P, Arlegui LE, Liesa CL, Simón JL (2012) Reply to the discussion by F Gutiérrez, P Lucha, J Guerrero, M Gutiérrez and D Carbonel on the article “Paleoseismological analysis of an intraplate extensional structure: the Concud fault (Iberian Chain, Spain)”. International Journal of Earth Science 101: 587-594. doi: 10.1007/s00531-011-0661-3.

Lafuente P, Arlegui LE, Liesa CL, Pueyo Ó, Simón JL (2014) Spatial and temporal variation of palaeoseismic activity at an intraplate, historically quiescent structure: The Concud fault (Iberian Chain, Spain). Tectonophysics 632: 167-187.

Liu J, Klinger Y, Sieh K, Rubin C (2004) Six similar sequential ruptures of the San Andreas fault, Carrizo Plain, California. Geology 32: 649–652.

Liu L, Zoback MD (1997) Lithospheric strength and intraplate seismicity in the New Madrid seismic zone. Tectonics 16: 585-595.

Martínez Solares JM, Cabañas L, Benito MB, Ribas A, Gaspar JM, Ruiz S, Rodríguez O (2013) Actualización de mapas de peligrosidad sísmica de España 2012.

Centro Nacional de Información Geográfica (CNIG), Madrid.

Maruyama T, Iemura K, Azuma T, Yoshioka T, Sato M, Miyawaki R (2007) Paleoseismological evidence for non-characteristic behavior of surface rupture associated with the 2004 Mid-Niigata Prefecture earthquake, central Japan. Tectonophysics 429: 45-60.

McCalpin JP (1996) Paleoseismology. Academic Press, New York.

McCalpin JP (2009) Paleoseismology, 2nd Edition: International Geophysics Series, Vol. 95, Elsevier Publishing.

Mezcua J, Martínez-Solares JM (1983) Sismicidad del Área Ibero-Mogrebí. IGN, Madrid.

Ministerio de Fomento (2002) Real Decreto 997/2002, de 27 de septiembre, por el que se aprueba la norma de construcción sismorresistente: parte general y edificación (NCSR-02). BOE 244: 35898-35967.

Moissenet E (1982) Le Villafranchien de la région de Teruel (Espagne). Stratigraphie-deformations-milieux. Colloque "Le Villafranchien méditerranéen", Lille, pp 229-253.

Opdyke N, Mein P, Lindsay E, Pérez-González A, Moissenet E, Norton VL (1997) Continental deposits, magnetostratigraphy and vertebrate paleontology, late Neogene of Eastern Spain. Palaeogeography, Palaeoclimatology, Palaeoecology 133: 129-148.

Pavlides S, Caputo R (2004) Magnitude versus faults´ surface parameters: quantitative relationships from the Aegean Region. Tectonophysics 380: 159–188.

Peña JL (1981) Las acumulaciones cuaternarias de la confluencia de los ríos Alfambra y Guadalaviar, en las cercanías de Teruel. Actas VII Coloquio de Geografía, Pamplona, pp 255-259.

Peña JL, Gutiérrez M, Ibáñez MJ, Lozano MV, Rodríguez J, Sánchez M, Simón JL, Soriano MA, Yetano LM (1984) Geomorfología de la provincia de Teruel. Instituto de Estudios Turolenses, Teruel.

Reid HF (1910) The Mechanics of the Earthquake, The California Earthquake of April 18, 1906, Report of the State Investigation Commission, Vol. 2, Carnegie Institution of Washington, Washington, D.C.

Rhoades DA, van Dissen RJ (2003) Estimates of the time-varying hazard of rupture of the Alpine Fault, New Zealand, allowing for uncertainties. New Zealand Journal of Geology and Geophysics 46: 479–488.

Roberts GP (1996) Noncharacteristic normal faulting surface ruptures from the Gulf of Corinth, Greece. Journal of Geophysical Research 101: 25255– 25267.

Roberts GP, Michetti AM, Cowie P, Nigel C, Morewood NC, Papanikolaou I (2002) Fault slip-rate variations during crustal-scale strain localisation, central Italy. Geophysical Research Letters 29 (8). doi: 10.1029/2001GL013529.

Roca E, Guimerà J (1992) The Neogene structure of the eastern Iberian margin: structural constraints on the crustal evolution of the Valencia trough (western Mediterranean). Tectonophysics 203: 203-218.

Rubio JC, Simón JL (2007) Tectonic subsidence v. erosional lowering in a controversial intramontane depression: the Jiloca basin (Iberian Chain, Spain). Geological Magazine 144: 1-15.

Sanz de Galdeano C, Peláez JA, López-Casado C (2003) Seismic potential of the main active faults in the Granada Basin (Southern Spain). Pure and Applied Geophysics 160: 1537-1556.

Schwartz DP, Coppersmith KJ (1984) Fault behaviour and characteristic earthquakes: Examples form the Wasatch and San Andreas Faults. Journal of Geophysical Research 89: 5681-5698.

Schwartz DP, Coppersmith KJ (1986) Seismic hazards: New trends in analysis using geologic data. In: Active Tectonics: Studies in Geophysics (RE Wallace, Chairperson), National Academic Press, Washington DC, pp 215–230.

Shimazaki K, Nakata T (1980) Time−predictable recurrence model for large earthquakes. Geophysical Research Letters 7: doi: 10.1029/GL007i004p00279.

Simón JL (1983) Tectónica y neotectónica del sistema de fosas de Teruel. Teruel 69: 21-97.

Simón JL (1989) Late Cenozoic stress field and fracturing in the Iberian Chain and Ebro Basin (Spain). Journal of Structural Geology 11: 285-294.

Simón JL, Lafuente P, Arlegui LE, Liesa CL, Soriano M.A (2005) Caracterización paleosísmica preliminar de la falla de Concud (fosa del Jiloca, Teruel). Geogaceta 38: 63-66.

Simón JL, Arlegui LE, Lafuente P, Liesa CL (2012) Active extensional faults in the central-eastern Iberian Chain, Spain. Journal of Iberian Geology 38: 127-144.

Simón JL, Pérez-Cueva AJ, Calvo-Cases A (2013) Tectonic beheading of fluvial valleys in the Maestrat grabens (eastern Spain): insights into slip rates of Pleistocene extensional faults. Tectonophysics 593: 73-84.

Simón JL, Arlegui LE, Ezquerro L, Lafuente P, Liesa CL (2014) Aproximación a la peligrosidad sísmica en la ciudad de Teruel asociada a la falla de Concud (NE España). Geogaceta 56: 7-10.

Stirling M, Rhoades D, Berryman K (2002) Comparision earthquake scaling relations derived from data of the instrumental and preinstrumental era. Bulletin of the Seismologic Society of America 92 (2): 820–830.

Wells DL, Coppersmith KJ (1994) New empirical relationships among magnitude, rupture length, rupture width, rupture area, and surface displacement. Bulletin of the Seismologic Society of America 84 (4): 974-1002.

Yeats RS, Sieh K, Allen CR (1997) The Geology of Earthquakes. Oxford University Press, New York.

Figure captions

Figure 1. Neogene-Quaternary extensional basins and main active faults in the central-eastern Iberian Chain. CaF: Calamocha fault; PF: Sierra Palomera fault; CoF: Concud fault; PoF: Pobo fault; FT: Teruel fault; VF: Valdecebro fault. Inset: location of the study area within the Iberian Peninsula. Location of figures 2 and 3 are shown.

Figure 2. Digital Elevation Model displaying epicenters of historical and instrumental earthquakes recorded in the Jiloca and Teruel grabens (DEM from SITAR, Aragón Regional Government). Seismic data from IGN (2010). The squared area includes historic and instrumental seisms computed in Fig. 12.

Figure 3. Geological map of the Concud Fault showing the location of the studied area. R1: Vallesian clastics (Rojo 1), with interbedded limestone and gypsum; P1: Turolian carbonates (Páramo 1); R2: Turolian clastics (Rojo 2); G2: Tortajada and Los Aljezares gypsum units; P2: Ruscinian carbonates (Páramo 2); R3: Villafranchian clastics and carbonates (Rojo 3); VP: Villafranchian pediment; T3: Early Pleistocene terrace; T2: Middle Pleistocene terraces; F: Middle-Late Pleistocene alluvial fans; T1: Late Pleistocene terraces and local pediments; T0: Holocene terrace.

Figure 4. Geologic cross section at the southern sector of the Concud Fault (see location in Fig. 5a).

Figure 5. (a) Detailed geological map of the southernmost sector of the Concud fault with location of the new (Mataueta) and previous (Masada Cociero) studied trenches (see location in Fig. 2). K: Upper Triassic; J: Lower Jurassic; R1a, R1b: Vallesian clastics (Rojo 1); L: Vallesian limestone; G1: Vallesian gypsum; P1: Turolian carbonates (Páramo 1); R3: Villafranchian clastics and carbonates (Rojo 3); T2: Middle Pleistocene terrace; T1a, T1b, T1c: Late Pleistocene terraces; P1a, P1b: Late Pleistocene pediments; A1a: Late Pleistocene alluvial infill; T0: Holocene terrace/flood plain. (b) Detailed topographic profile across the surveyed fault scarp in pediment P1b. (c) Field aspect of P1b alluvial deposits overlying T1b fluvial deposits.

Figure 6. Detailed log of the Mataueta trench showing location of samples for OSL dating. Black, bold case: OSL ages considered for paleoseismic reconstruction; grey: non-reliable, rejuvenated ages.

Figure 7. Detailed trench view of the main fault zone (cell C18 and neighbouring ones, see location in Fig. 6), and stereoplot showing the orientation of measured fault planes.

Figure 8. Proposed evolutionary model at the Mataueta trench from retrodeformational analysis.

Figure 9. Synthesis of paleoseismic interpretation at the Mataueta trench and estimation of coseismic throw values. Labels 1 to 5: sedimentary units. Fα, Fβ, Fγ, Fδ faults activated during seismic events. Solid triangle, square and circle: tip points for the base of units 2, 3 and 4, respectively (using smoothed envelopes); open triangle, square and circle: virtual tip points at the hanging-block for the same markers extrapolated over the central graben. T_x, T_y, T_z: observed coseismic throws for events X_M, X_M, X_M, respectively. TT_2, TT_3, TT_4: real tectonic throws for three sedimentary markers (base of units 2, 3 and 4, respectively). Real tectonic throws for individual events (TT_x, TT_y, TT_z) are obtained as: $TT_x = TT_2 - TT_3 = 1.4$ m; $TT_y = TT_3 - TT_4 = 0.7$ m; $TT_z = TT_4 = 2.2$ m.

Figure 10. Integrated paleoseismic history of the Concud Fault including events recorded at the Mataueta trench and those interpreted in the previous trenches. (1) Lafuente 2011; Lafuente et al. 2011a; (2) Lafuente 2011; Lafuente et al. 2014. Time constraints on which correlation is based are indicated in detail.

Figure 11. Slip history of the Concud Fault, as inferred from the overall palaeoseismic results. The average slip rate for the whole recorded activity period, as well as for three successive stages, are indicated.

Figure 12. Frequency-magnitude diagram for the historical and instrumental seismic activity in the Teruel area (squared in Fig. 2), showing a log-linear relationship that fits the parameters of the characteristic earthquake of the Concud Fault. Modified from Simón et al. (2014).

Table captions

Table 1. Results of absolute OSL dating of samples collected at the Mataueta trench, as well as in a neighbouring fluvial terrace (T1c sublevel) offset by the Concud Fault. The samples were analysed in Laboratorio de Datación y Radioquímica, Universidad Autónoma de Madrid, Spain. The supralinearity value in every sample is 0 Gy. Sedimentary unit, material and cell location of samples are also shown (see also Fig. 6). Asterisks represent ages with a likely rejuvenation process.

Table 2. Ages and throws for events distinguished in Mataueta trench.

Table 3. Results of probabilistic seismic hazard assessment for the characteristic earthquake of the Concud Fault. Owing to the uncertainty about the age of the youngest event, three distinct hypothetic values have been considered.

Figure 01
Click here to download Figure: Fig 01.tif

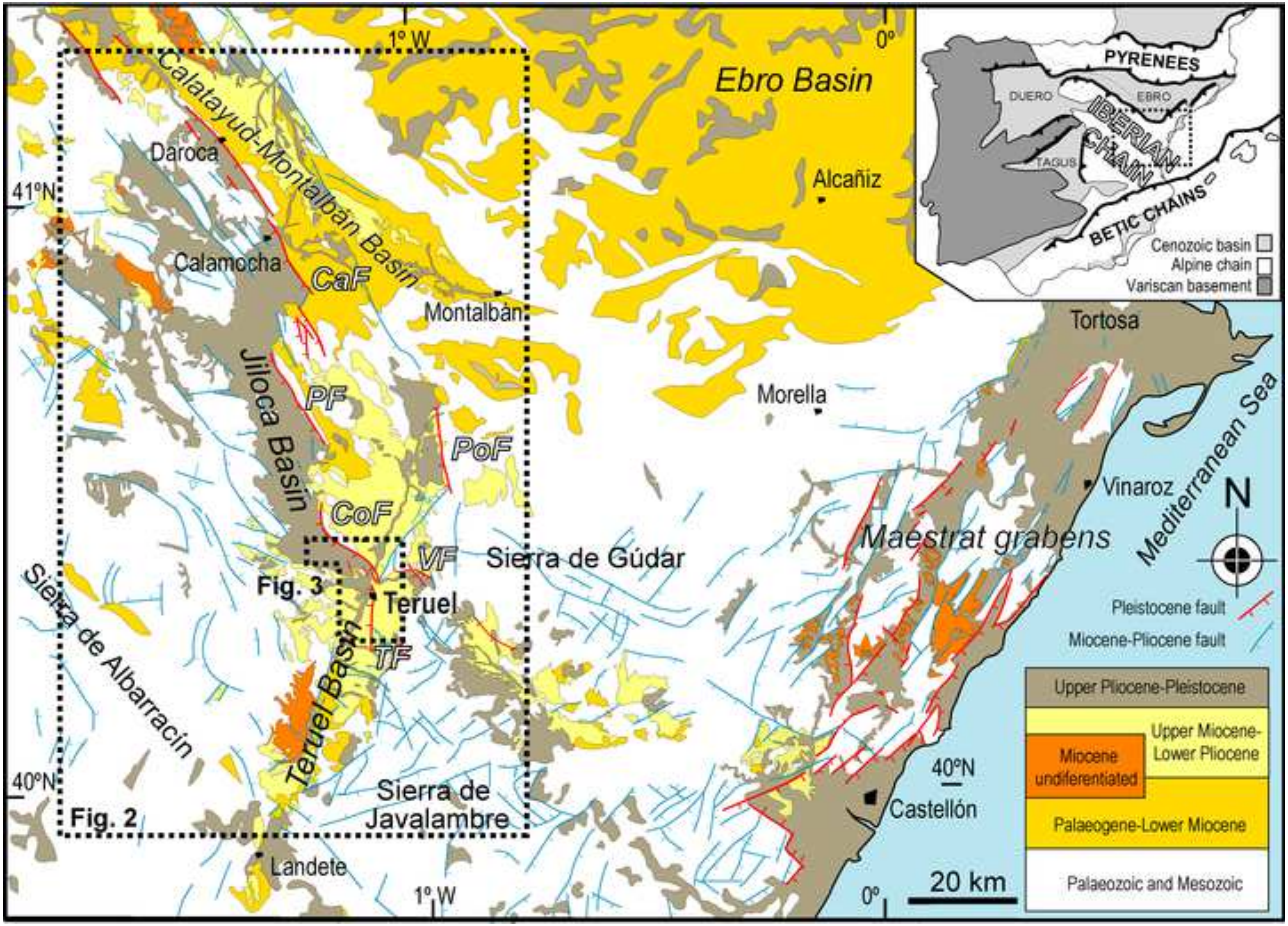

Figure 02

Click here to download Figure: Fig 2.tif

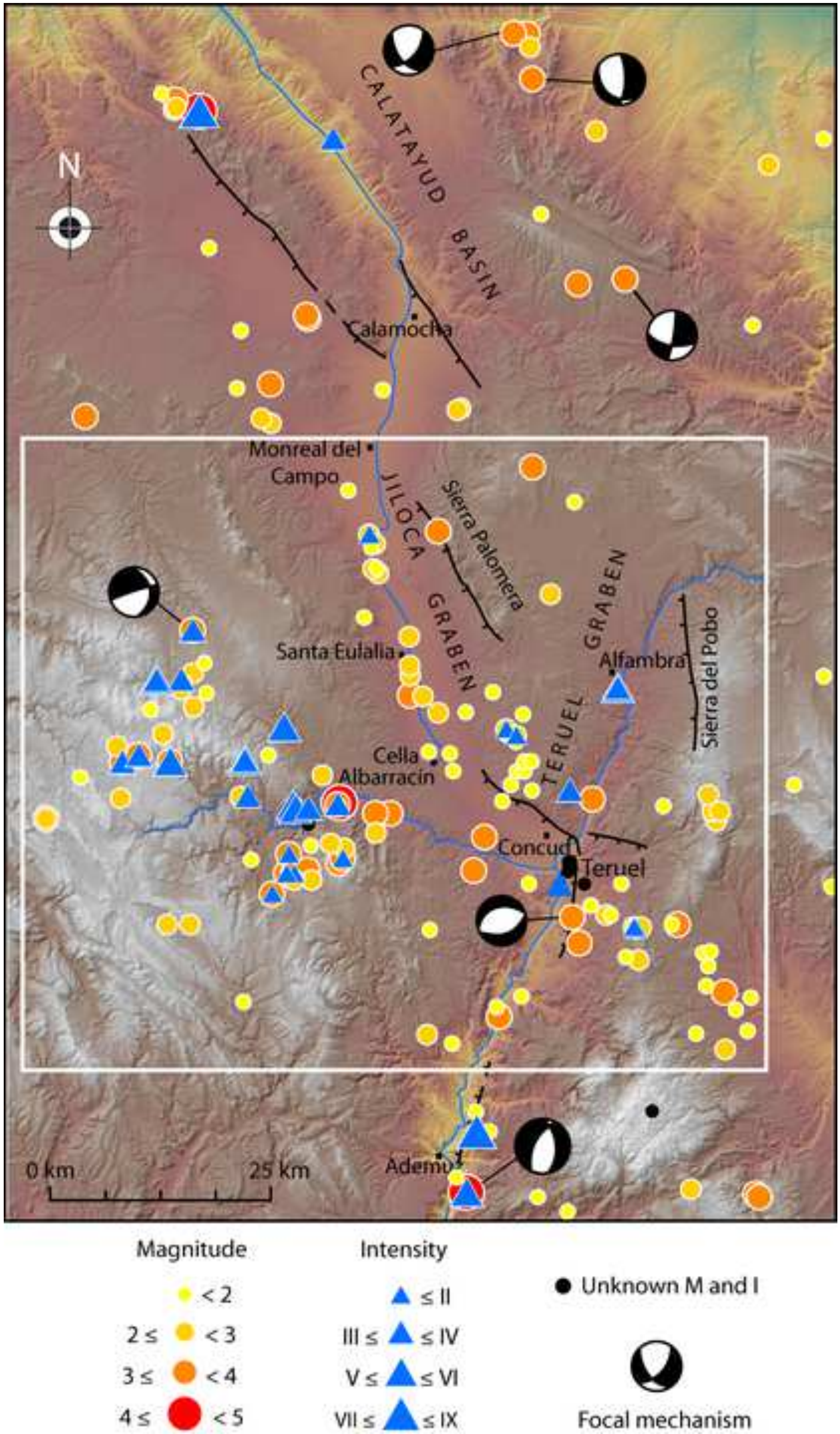

Figure 03
Click here to download Figure: Fig 03.tif

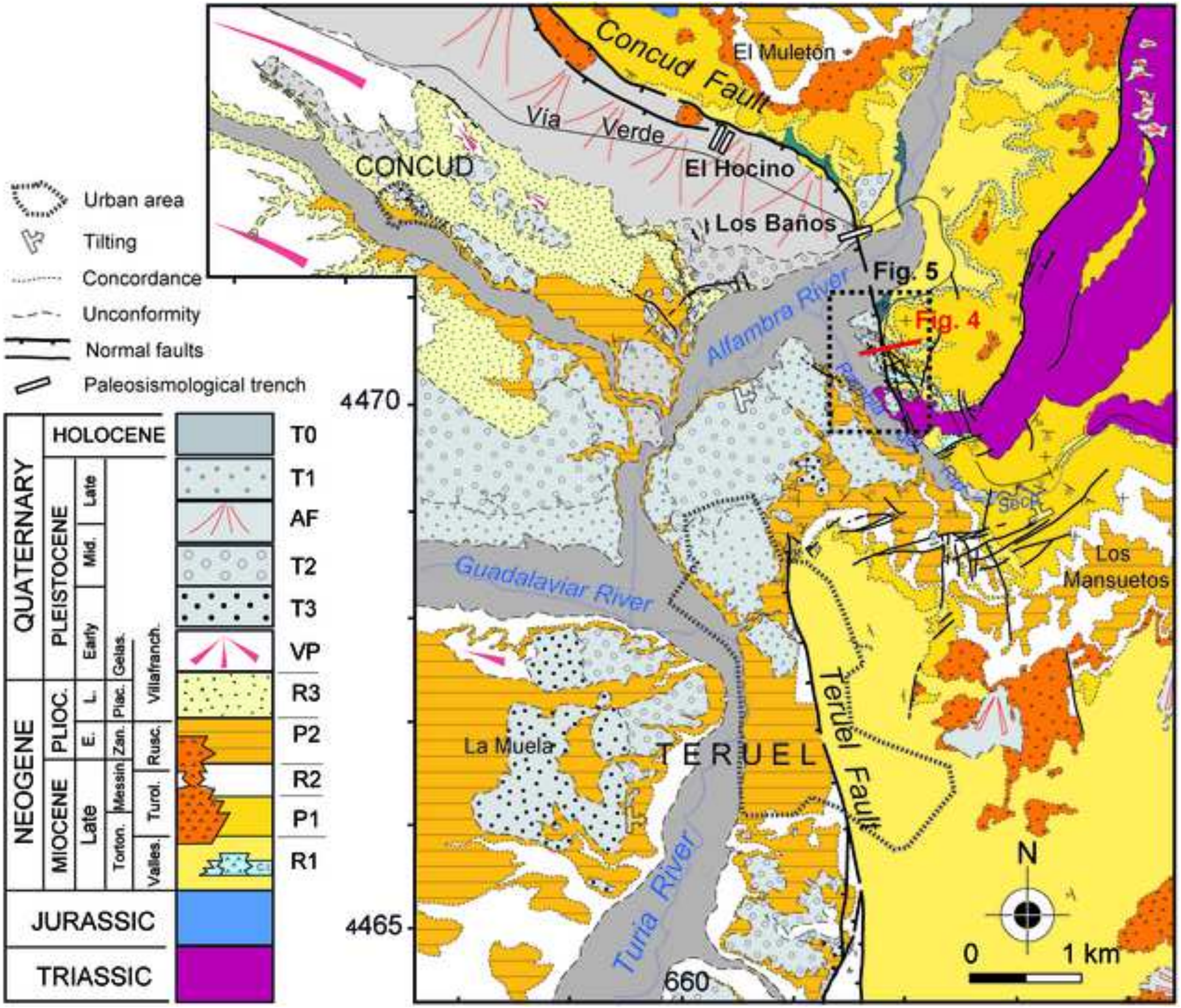

Figure 04
Click here to download Figure: Fig 04.tif

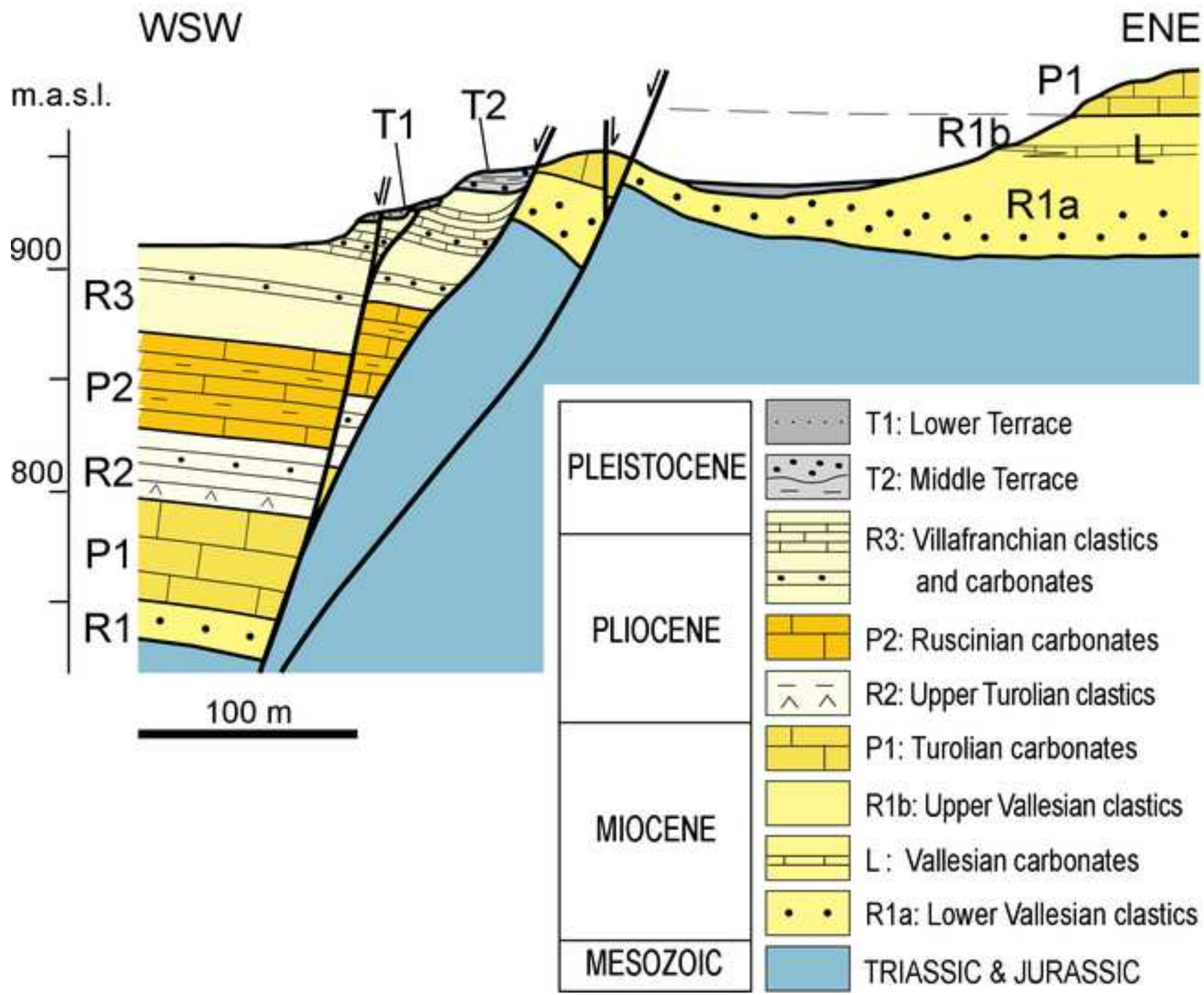

Figure 5

Click here to download Figure: Figure 5.tif

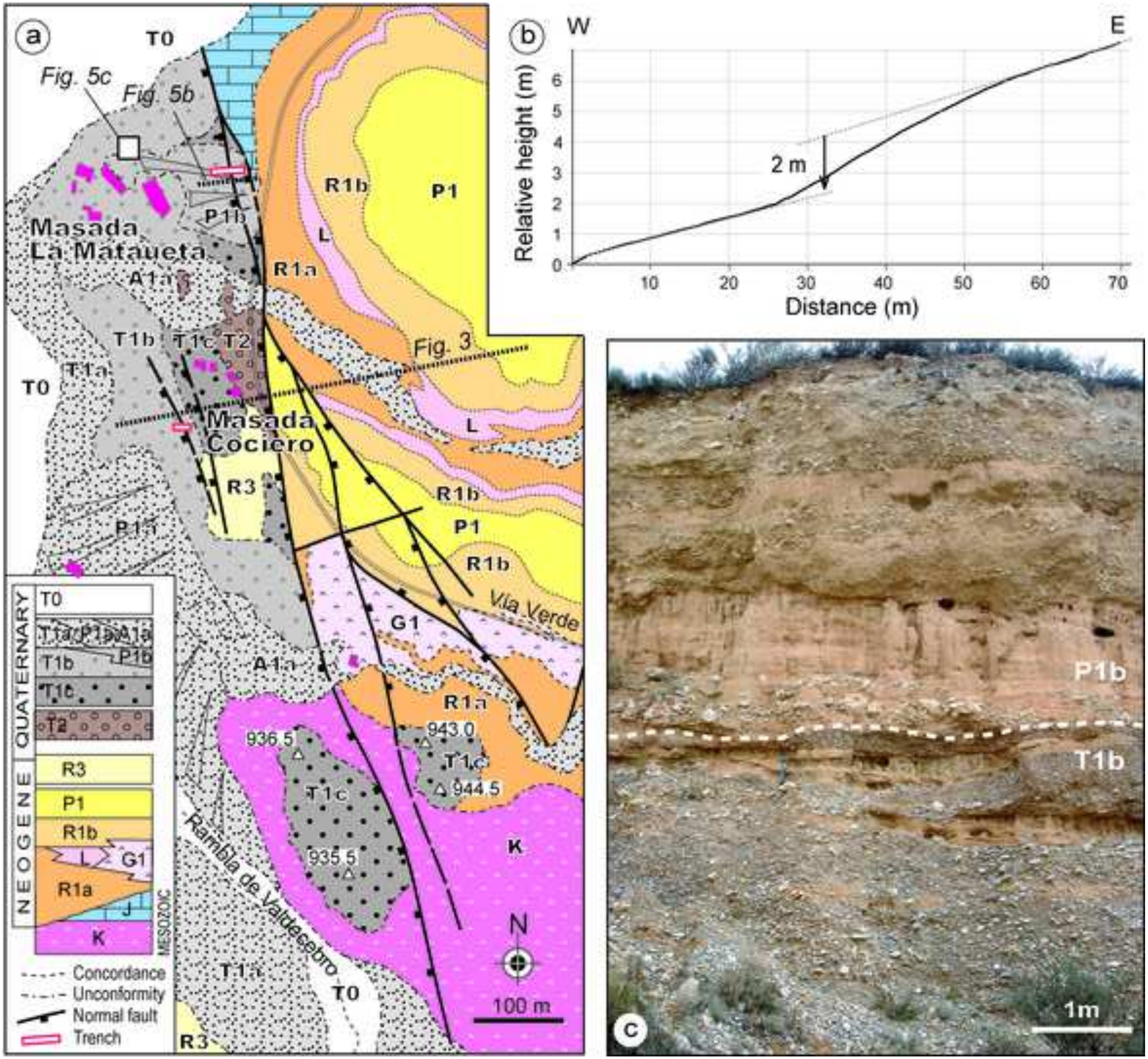

Figure 6

Click here to download Figure: Figure 6.tif

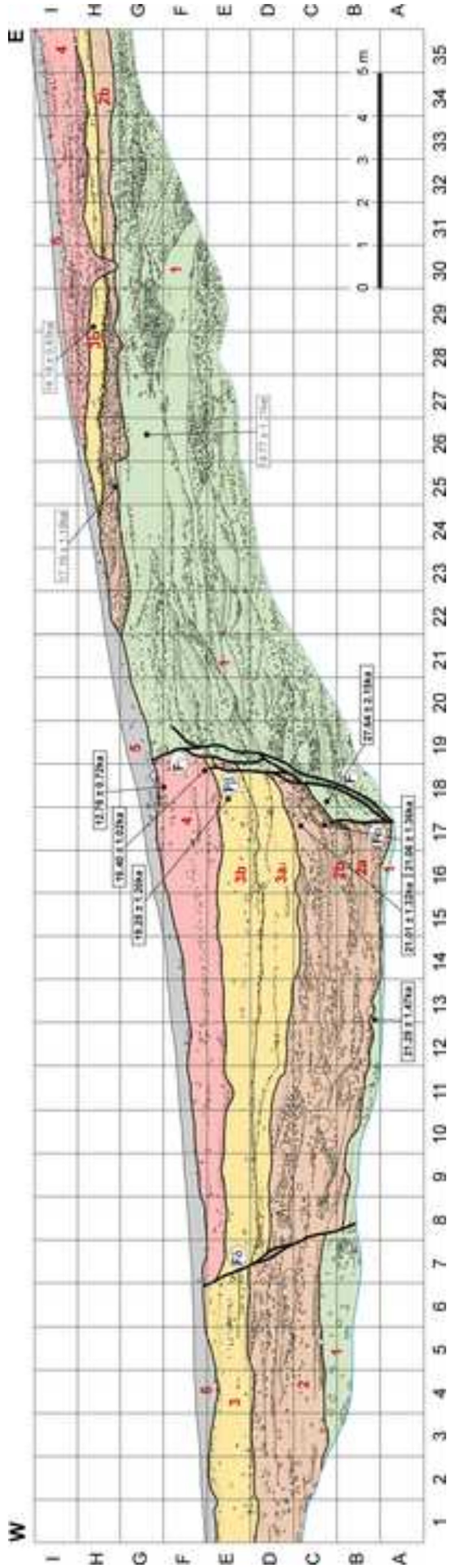

Figure 07
Click here to download Figure: Fig 07.tif

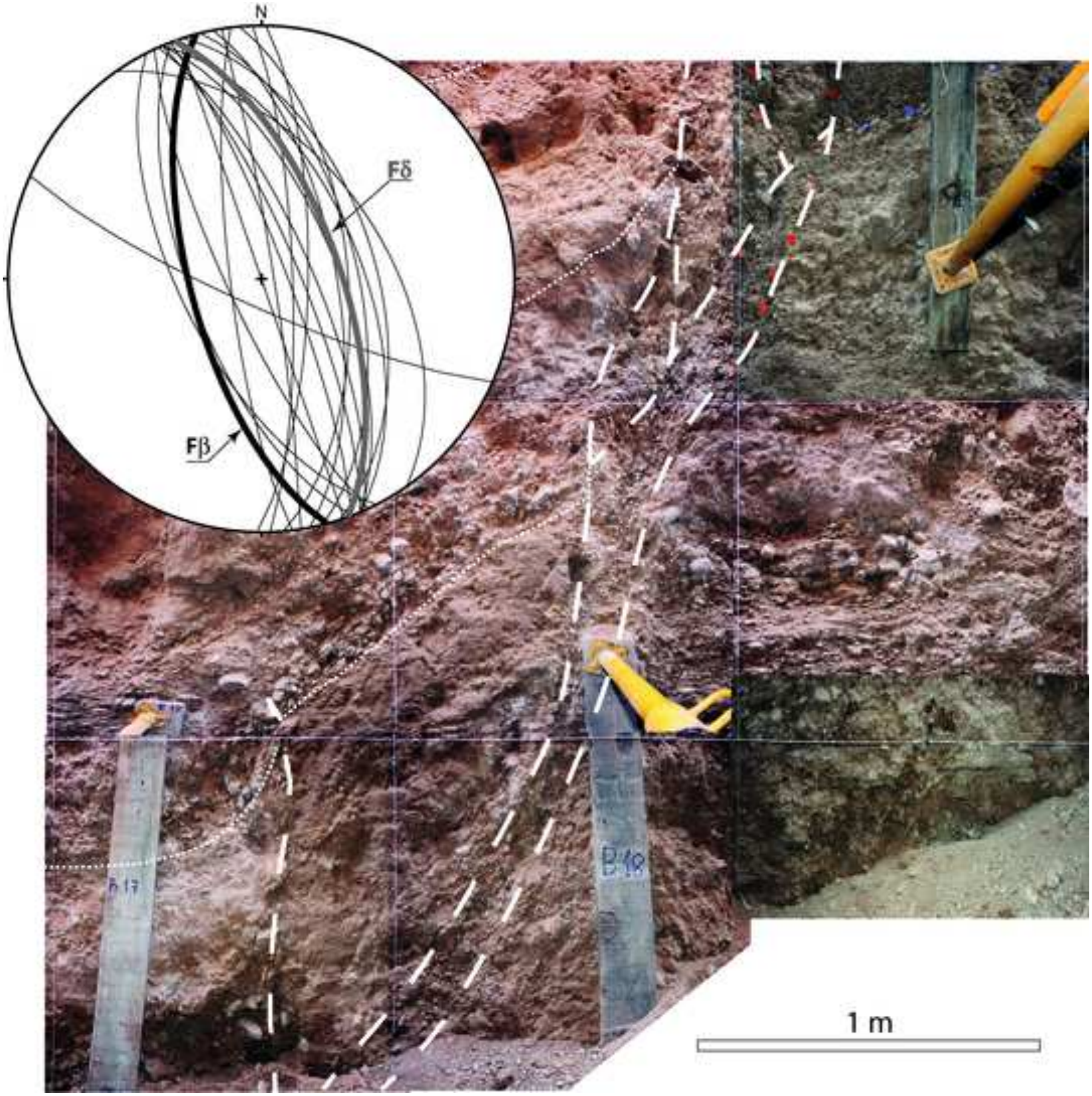

Figure 8
Click here to download Figure: Figure 8.tif

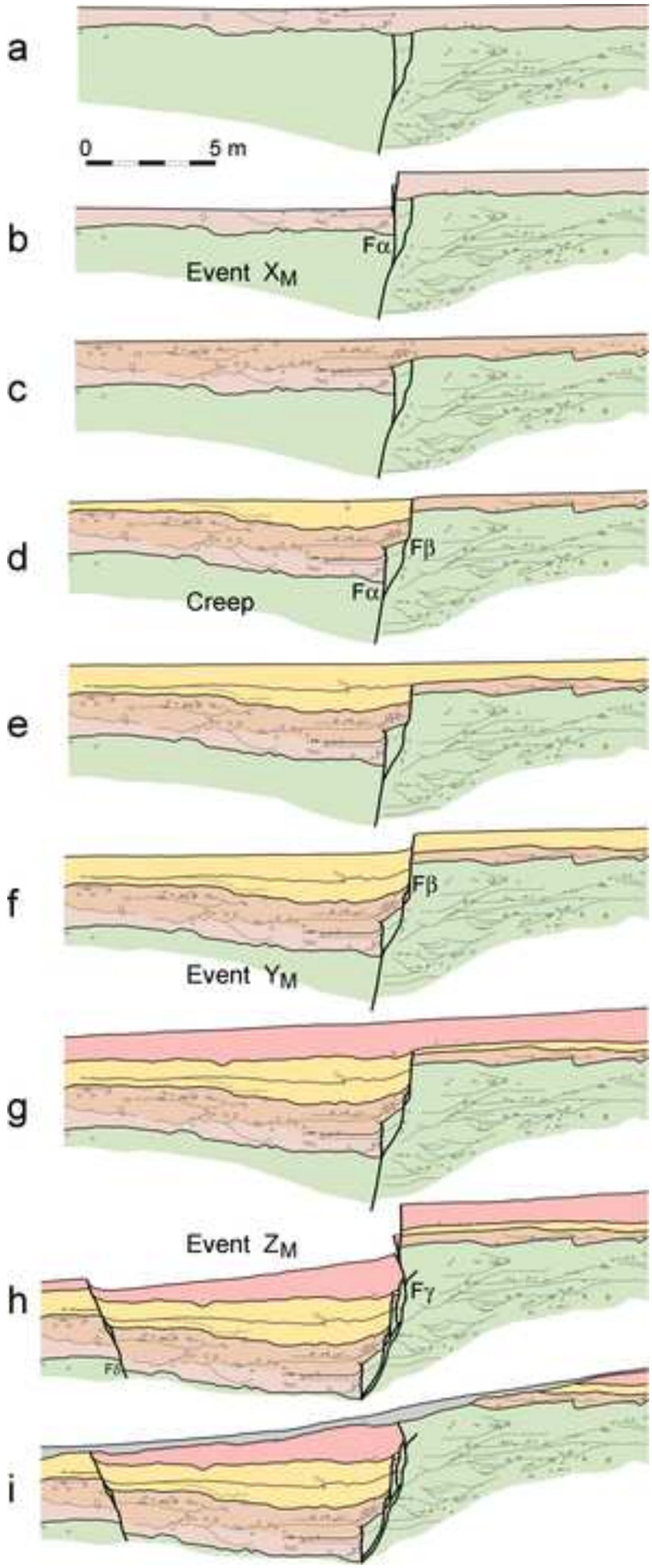

Figure 09

Click here to download Figure: FIG 09 def.tif

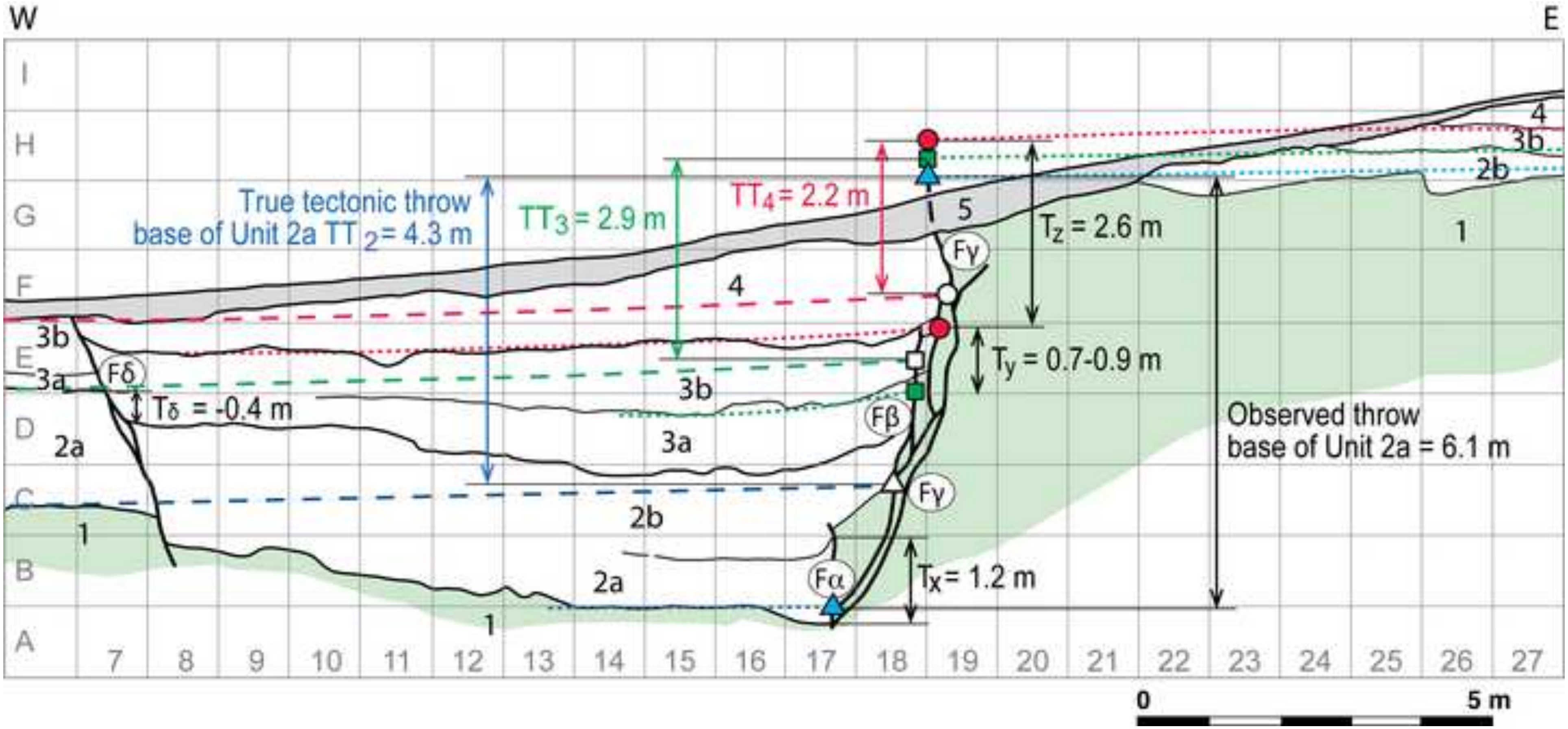

Figure 10

Click here to download Figure: Figure 10.tif

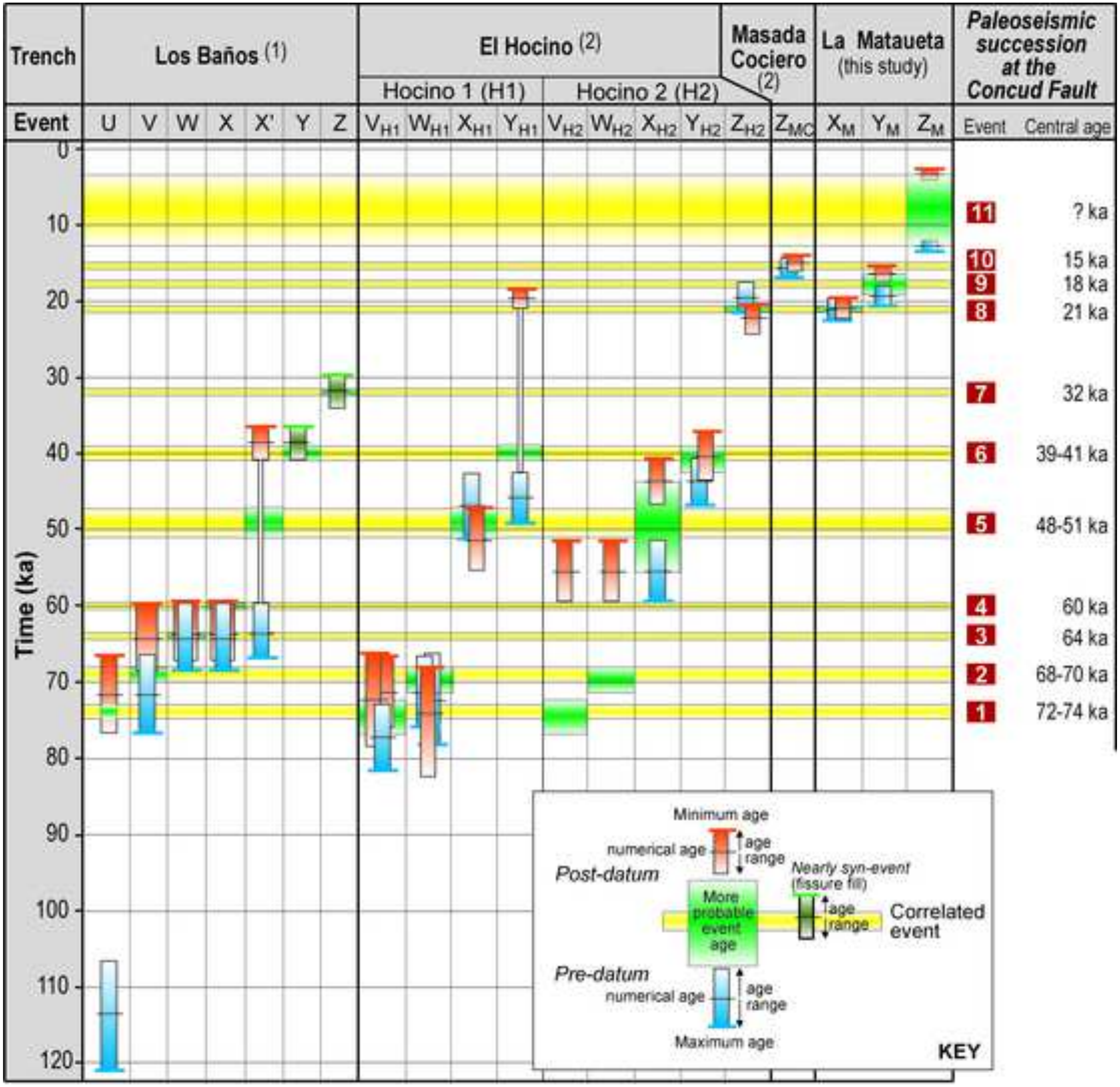

Figure 11
Click here to download Figure: FIG 11 def.tif

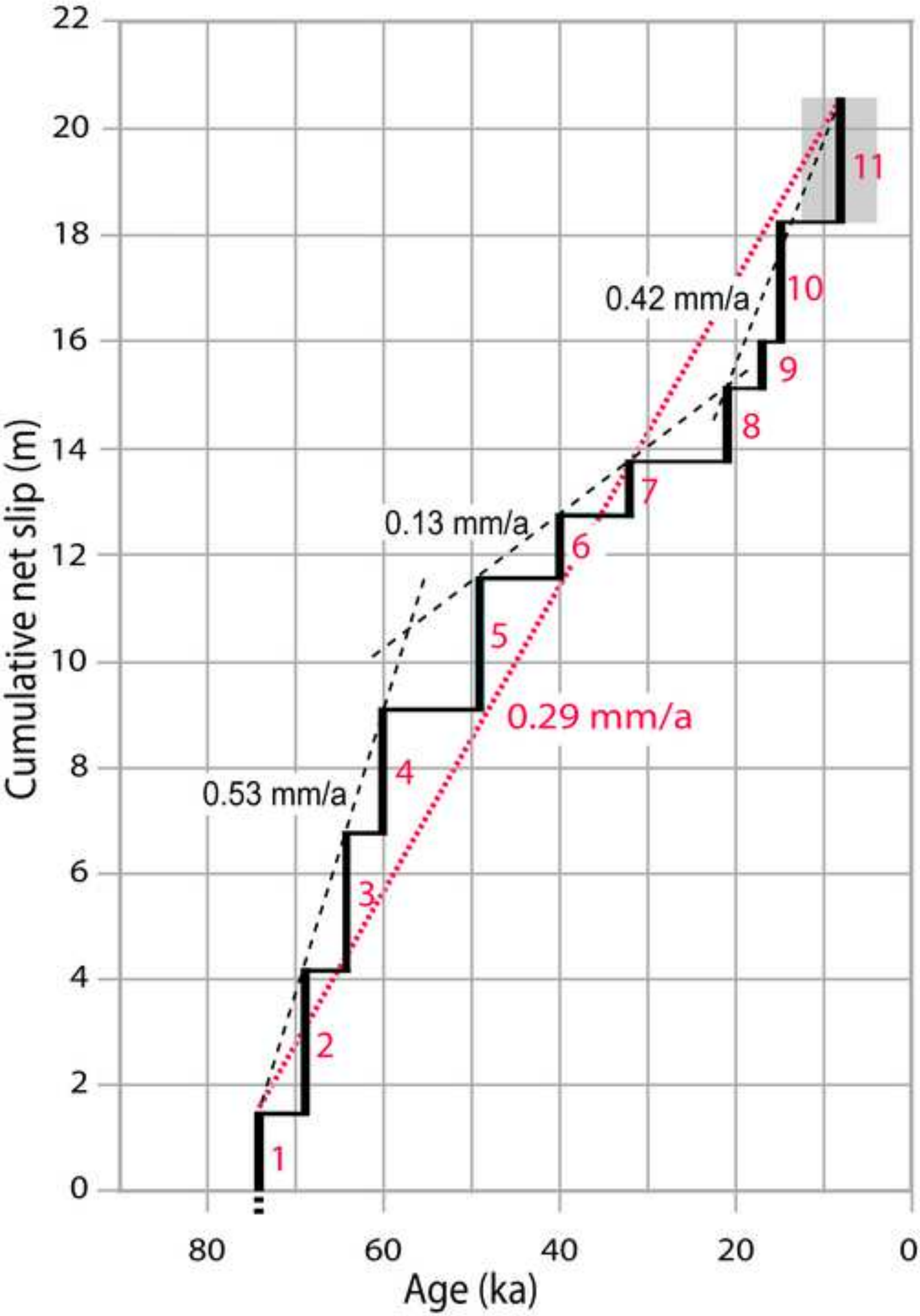

Figure 12

Click here to download Figure: FIG 12 def.tif

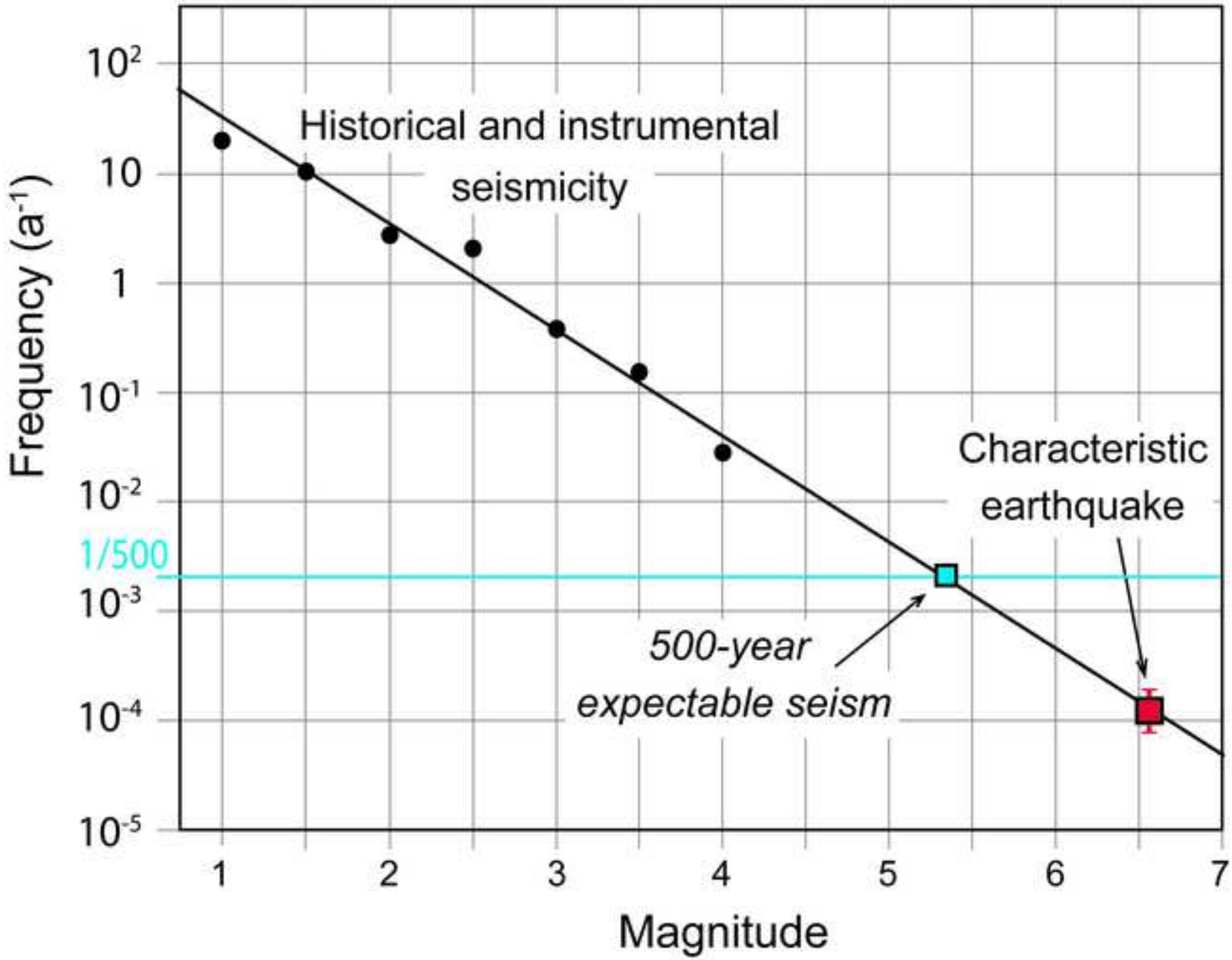

Table 1
Click here to download Table: Table 1.doc

Laboratory Reference	Equivalent dose (Gy)	Annual dose (mGy/yr)	K Factor	OSL age (years B.P.)	Sedimentary Unit	Material	Location (cell in Fig. 5)
Hanging-wall block							
MAD-6164rBIN	39.18	1,84	0.12	21,293 ± 1,479	Unit 1 (top)	Silt-sand	B-13
MAD-6135SDA	36.240	1.72	0.10	21,069 ± 1,368	Unit 2 (middle part)	Sand	C-17I
MAD-6160SDA	43.51	2.07	0.11	21,019 ± 1,329	Unit 2 (top)	Coarse sand	C-17s
MAD-6137SDA	47.76	2.48	0.15	19,258 ± 1,207	Unit 3 (top)	Silt-sand	E-18R
MAD-6133SDA	36.25	2.21	0.12	16,402 ± 1,022	Unit 4 (bottom)	Silt	F-18
MAD-6134SDA	34.14	2.67	0.13	12,786 ± 723	Unit 4 (top)	Sand	G-18
Fault zone (between faults α and β)							
MAD-6136SDA	97.58	3.53	0.47	27,643 ± 2,158 *	Unit 1 (top)	Lutite-silt	C-18
Footwall block							
MAD-6163rBIN	49.19	2.62	0.16	18,774 ± 1,213 *	Unit 1 (top)	Silt-sand	G-26
MAD-6161rBIN	49.78	2.90	0.10	17,165 ± 1,194 *	Unit 2+3 (bottom)	Sand with pebbles	H-25
MAD-6138SDA	40.14	2.83	0.18	14,183 ± 835 *	Unit 2+3 (top)	Silt-sand	H-29
T1c fluvial terrace (footwall block outside the trench)							
MAD-5778rpSDA	48.67	2.21	0.08	22,022 ± 1,629	Fluvial terrace	Sand	-

Table 1. Results of absolute OSL dating of samples collected at the Mataueta trench, as well as in a neighbouring fluvial terrace (T1c sublevel) offset by the Concud fault. The samples were analysed in Laboratorio de Datación y Radioquímica, Universidad Autónoma de Madrid, Spain. The supralinearity value in every sample is 0 Gy. Sedimentary unit, material and cell location of samples are also shown (see also Fig. 6). Asterisks represent ages with a likely rejuvenation process (see text for explanation).

Table 2

Event	Apparent throw in main fault zone (m)		Real tectonic throw (m)		Net slip (m)	Age (ka BP)		
						Predating	Postdating	Most probable
X_m	T_x	> 1.2	TT_x	1.4	1.5	21.3 ± 1.5	21.0 ± 1.4	21.0
'Creep-like' stage		1.1 -1.4				21.0 ± 1.3	19.2 ± 1.2	21.0 to 19.2
Y_m	T_y	0.7 - 0.9	TT_y	0.7	0.8	19.2 ± 1.2	16.4 ± 1.0	ca. 18.0
Z_m	T_z	2.6	TT_z	2.2	2.4	12.8 ± 0.7	-	post 12.8
Total		5.6 – 6.1		4.3	4.7			

Hypothetic elapsed time (ka)	Interseismic period (average ± standard deviation, ka)	Probability of occurrence (%) of characteristic earthquake (M = 6.5-6.6) in a 500 years term
13.5	7.1 ± 3.5	26.1
8	7.3 ± 2.7	19.3
2.7	8.0 ± 3.3	2.3